The role of microbial sulfate reduction in calcium carbonate polymorph selection

Chin Yik Lin[1], Alexandra V. Turchyn[1], Zvi Steiner[1], Pieter Bots[2], Giulio I. Lampronti[1], Nicholas J. Tosca[3]

[1]Department of Earth Sciences, University of Cambridge, Downing Street, Cambridge CB2 3EQ, United Kingdom.

[2]Department of Civil and Environmental Engineering, University of Strathclyde, Glasgow G11XJ, United Kingdom.

[3]Department of Earth Sciences, University of Oxford, South Parks Road, Oxford OX1 3AN, United Kingdom.

ABSTRACT

Microbial sulfate reduction is a dominant metabolism in many marine sedimentary environments. The influence of this metabolism on the kinetics of $CaCO_3$ growth, as well as the dominant polymorphs precipitated, is poorly understood. To investigate the role of microbial metabolism on $CaCO_3$ precipitation and polymorph selection, we conducted growth experiments with the sulfate reducing bacteria (*D. bizertensis*) in media with varying Mg/Ca and different seeding materials (calcite and kaolinite). Our results suggest that sulfate reducing bacteria both induce carbonate mineral precipitation through an increase in alkalinity and serve as a nucleation sites for the growing carbonate mineral; the majority of the carbonate minerals produced were on cell material rather than mineral seeds. We also find the Mg/Ca and presence of phosphate in the media play a key role in controlling the rates of carbonate mineral precipitation and calcium carbonate polymorph selection. In media where the Mg/Ca is greater than 2, crystalline monohydrocalcite (MHC) is the primary carbonate mineral produced. Although phosphate concentrations have a lesser effect on which polymorph initially precipitates, a series of transformation experiments suggests that the presence of phosphate stabilizes MHC crystals and prevents its transformation to more stable calcium carbonate polymorphs. Collectively, these results suggest that the polymorph of microbially-mediated calcium carbonate cements is determined by the solution chemistry upon nucleation.

Keywords: monohydrocalcite; Mg/Ca, seeding material, phosphate, transformation, sulfate reducing bacteria, incubation, inhibitors, nucleation

1.0 INTRODUCTION

Microbial sulfate reduction, coupled either to organic matter oxidation or anaerobic methane oxidation, is one of the key microbial reactions driving sedimentary carbonate formation in marine sediments, intertidal marshes, and hypersaline lakes (Berner et al., 1970; Pye et al., 1990; Coleman et al., 1993; Visscher et al., 2000; Warthmann et al., 2000; Raiswell and Fisher, 2004; Baumgartner et al., 2009; Gallagher et al., 2012; Meister, 2013). Microbial sulfate reduction, particularly followed by precipitation of sedimentary pyrite, raises pH and increases alkalinity, while the negatively charged bacterial cell surface can serve as a nucleation surface for carbonate/mineral growth (Dong et al., 2000; van Lith, 2001; Bosak and Newman, 2005; Visscher and Stolz, 2005; Aloisi et al., 2006; Wacey et al., 2007; Zhu and Dittrich, 2016; Picard et al., 2018). The production of exopolymeric substances (EPS) around the bacterial cells also aids the nucleation and subsequent precipitation of calcium carbonate (Kawaguchi and Decho, 2002; Braissant et al., 2007; Dupraz et al., 2009; Obst et al., 2009; Tourney and Ngwenya, 2009; Balci et al., 2018). Despite work on the process of microbially-induced carbonate mineral precipitation, our understanding of how microbial sulfate reduction influences calcium carbonate mineralization and the formation of various calcium carbonate polymorphs remains limited. The vast majority of studies exploring the formation of different calcium carbonate polymorphs have focused on abiotic precipitation experiments, despite the fact that the majority of natural calcium carbonate mineral precipitation is biologically controlled.

The earliest studies on the nucleation, crystallization, and transformation of various calcium carbonate polymorphs focused largely on the precipitation of aragonite versus calcite and the role of magnesium ions and Mg/Ca ratio of the solution (Katz, 1973; Berner, 1975; Burton, 1993; Ries et al., 2008; Smeets et al., 2015). It was initially shown that the precipitation of aragonite is favoured in a high ionic strength solution with high Mg/Ca ratio (Mg/Ca > 1), while calcite is favoured in solutions with a lower Mg/Ca ratio (Mg/Ca < 1). The important role of magnesium in promoting different calcium carbonate polymorphs derives from the fact that magnesium possesses greater hydration energy and therefore promotes the formation of

hydrous carbonate phases (Christ and Hostetle, 1970; Lippman, 1973; Ries et al., 2008; de Choudens-Sanchez and Gonzalez, 2009; Politi et al., 2009; Tommaso and de Leeuw, 2010; Hopkinson et al., 2012; Nishiyama et al., 2013; Blue et al., 2017). In addition, there is also a fundamental energetic barrier imposed by magnesium substitution for calcium in the calcite lattice, which may in part kinetically inhibit the formation of Mg-rich calcium carbonate minerals (Elstnerova et al., 2010; Xu et al., 2013).

Most inorganic precipitation studies have also shown that if the initial calcium carbonate precipitate is metastable (e.g. amorphous calcium carbonate or monohydrocalcite (MHC)), it will transform to calcite or aragonite over time via the Ostwald step rule and/or other non-classical nucleation pathways (Munemoto and Fukushi, 2008; Bots et al., 2012; Liu et al., 2013; Rodriguez-Blanco et al., 2014; De Yoreo et al., 2015). However, the transformation mechanisms of amorphous calcium carbonate or MHC in natural environments are still poorly understood (Stoffers and Fischbeck, 1974; Dahl and Buchardt, 2006; Nishiyama et al., 2013; Ihli et al., 2014; Munemoto et al., 2014; Wolf et al., 2015; Meic et al., 2017). To constrain the behavior of these transient intermediate polymorphs, laboratory studies have been performed under both dry and wet conditions (Marschner, 1969; Hull and Turnbull, 1973; Kamiya et al., 1977; Dejehet et al., 1999; Liu et al., 2013). MHC has been reported to transform to aragonite in a heated atmosphere (Brooks et al., 1950; Kamiya et al., 1977), to calcite in a magnesium-free medium (Taylor, 1975) and to aragonite in media with $Mg^{2+}/(Ca^{2+} + Mg^{2+})$ greater than 20 mol% (Munemoto and Fukushi, 2008). Although these inorganic and abiotic studies have highlighted several variables that can influence calcium carbonate mineralisation and polymorphism, microbial systems involve a number of interconnected processes that may affect carbonate mineralization in unanticipated ways. This may obscure the influence of specific metabolic processes on calcium carbonate formation in sediments, and the attendant biogeochemical consequences.

Understanding the dominant calcium carbonate polymorph produced through microbially-induced carbonate mineral precipitation is inherently more difficult because microbial metabolic byproducts and solution chemistry evolve over time. Within sedimentary pore fluids, for example, the concentrations of various elements that may promote or inhibit carbonate precipitation or play a role in the type of polymorph precipitated, may change with

depth and/or time. For example, dissolved phosphate concentrations, which have been shown to influence carbonate polymorphism, can range from 0 – 600 uM in sediment pore waters (Delaney, 1998; Burdige, 1991; Sasaki et al., 2001; Faul et al., 2005; Kraal et al., 2012; Sinkko et al., 2013; Stockmann et al., 2018). An unanswered question is whether during microbially-induced carbonate mineral formation there is a difference in the calcium carbonate polymorphs produced, relative to those found in the well-studied abiotic experiments. If so, what are the master variables that influence the stability field of the precipitating carbonate polymorph?

In this paper, we explore how microbial sulfate reduction influences calcium carbonate polymorphism using pure cultures of sulfate reducing bacteria under varying Mg/Ca and with different seeding materials. We also investigate the transformation of the microbially induced calcium carbonate polymorphs to more stable polymorphs under a range of geochemical conditions. Finally, we propose a stability field for calcium carbonate polymorphs obtained from our experiments and suggest the master variables that control the formation of microbially-induced calcium carbonate polymorphs.

2.0 EXPERIMENTAL

2.1 *Incubation* experiments

A pure culture of the sulfate reducing bacteria *Desulfovibrio bizertensis* (single bacteria strain) was used in all incubation experiments. The strain was purchased from Leibniz-Institut DSMZ-Deutche Sammlung von Mikroorganismen und Zellkulturen GmbH (DSMZ) DSM No. 18034. This strain was originally isolated from marine sediments in the Mediterranean Sea near Bizerte, Tunisia (Haouari et al., 2006). Our incubations were carried out in either 125 mL or 100 mL reaction vessels, tightly sealed with a blue butyl rubber stopper under strictly anoxic conditions. All experiments were performed at 25 ± 1°C in a water bath incubator. The incubation experiments were performed with different Mg/Ca (0:1, 1:1; 2:1, 3:1, 4:1 5.2:1; 9:1) including Atlantic seawater and artificial seawater and different seeding materials (kaolinite and calcite – see below).

2.2 *Composition of culture medium and inoculation*

The bacteria were initially cultured in Medium 163 as recommended by DSMZ (Supplementary A). An inoculum of the bacteria at stationary phase was transferred into the modified media and grown three times before the experiment began. The recipe for DSMZ medium 163 and the seawater medium used in this study are given in full in Supplementary Materials B. Artificial seawater was prepared using the Standard Practice for the Preparation of Substitute Ocean Water – Designation: D1141-98 (Reapproved 2013). Stock solutions of artificial seawater were freshly made from analytical grade (Analar) reagents and diluted to the desired Mg/Ca ratio. The seawater solution was heated to approximately 80 °C for two hours to degas O_2. Then, the solution was allowed to cool and the above chemicals were added except yeast extract. Formate (7.5 g L^{-1} or 110 mM HCOO-Na) was used as the sole electron donor in this study. Approximately 0.01% w/v of reductants (ascorbic acid and Na-thioglycolate), 4.0% w/v yeast extract and 1 mg L^{-1} resazurin (oxygen indicator) were added into both the Atlantic seawater and artificial seawater medium. About 80 mL of the solution was then decanted into smaller incubation vials with 0.3 g of seeding materials (such as calcite or kaolinite), crimp sealed and flushed with 90% N_2/10% CO_2 gas for 30 minutes. Finally, the medium was autoclaved for 15 minutes at 121°C. The sample medium was subsequently cooled to 25°C in the water bath before being inoculated. Yeast extract solution was added to the medium using a syringe filter (0.2 µm) before inoculation. Control samples were immediately re-autoclaved after inoculation to kill the bacteria, then placed into the water bath. All results from the control experiments are given in the supporting online material.

2.3 *Biotic incubation experiment*

Three sets of incubation experiments were undertaken with varying Mg/Ca and seeding materials (Table 1). Approximately 0.3 g of seeding material was used. Biotic incubation experiments were performed without stirring. Experiments were sampled every few days until carbonate precipitated – which was identified during the incubation based on a coincident decrease in pH and calcium concentration. Details of abiotic experiments are reported in Supplementary Material C.

Table 1: Summary of experiment setup for biotic incubation experiments.

Experiment	Mg^{2+} (mM)	Ca^{2+} (mM)	Mg/Ca	Seeds
K-0:1	0	10	0	Kaolinite
C-0:1	0	10	0	Calcite
K-0:2	0	20	0	Kaolinite
C-0:2	0	20	0	Calcite
K-1:1	10	10	1	Kaolinite
C-1:1	10	10	1	Calcite
K-2:2	20	20	1	Kaolinite
C-2:2	20	20	1	Calcite
K-3:3	30	30	1	Kaolinite
C-3:3	30	30	1	Calcite
K-4:4	40	40	1	Kaolinite
C-4:4	40	40	1	Calcite
K-2:1	20	10	2	Kaolinite
C-2:1	20	10	2	Calcite
K-3:1	30	10	3	Kaolinite
C-3:1	30	10	3	Calcite
K-4:1	40	10	4	Kaolinite
C-4:1	40	10	4	Calcite
K-Atl-SW	52	10	5.2	Kaolinite
C-Atl-SW	52	10	5.2	Calcite
K-9:1	90	10	9	Kaolinite
C-9:1	90	10	9	Calcite

2.4 *Aqueous sample analysis*

Media was collected from the sample bottle over the course of the experiments using a sterilized needle and syringe and without shaking the vials. Samples were filtered using a 0.2 µm filter and analyzed for alkalinity, sulfide concentration, major cations (calcium, magnesium, sodium, and potassium) and anions (sulfate and chloride). The pH was measured at 25°C on the NBS scale using an Orion 3 Star meter with ROSS micro-electrode (ORION 8220 BNWP PerpHect ROSS – platinum wire as reference in iodine/potassium iodide solution, ROSS

internal filling solution is 3M KCl). Samples for alkalinity, anions and cations were filtered through a 0.2 um syringe filter. Alkalinity was titrated potentiometrically with 0.1 M of HCl using a Metrohm 848 Titrino plus with error of 2.5%. The HCl used for titrations was standardized with certified reference material (CRM) 2.2298 meq/L. The CRM batch #157 used was provided by A.G. Dickson of Scripps Institution of Oceanography (Dickson et al., 2003).

An unfiltered sample was centrifuged at 900 rpm to separate any suspended solid in the solution before measurement for Optical density (OD) at 600 nm spectrum in a AquaMate Plus UV-VIS spectrophotometer. Phosphate concentrations were measured on the spectrophotometer using the molybdivanadophosphoric acid method (at 380 nm) described in Kitson and Mellon (1944).

Major cations and anions were diluted 20 times before being measured using ion chromatography on a Dionex ICS-5000^{+} SP. The cation concentrations were obtained with column IonPac AS18 and methanesulfonic acid (MSA 30mM) >99% as the eluent. The anions were passed through an anion column IonPac AG18 with 31mM of potassium hydroxide (KOH) as eluent. Calibration standards were prepared by dilution of OSIL Atlantic Seawater standard into 2%, 5% and 10% solution for all batch of analyses.

2.5 *Solid phase analysis*

The experiments were killed immediately after the final sampling. The sample (both solid and aqueous parts of the experiments) were decanted into a 50 mL falcon tube which was centrifuged at 5000 rpm for five minutes. Then, the solution was discarded. The remaining solid samples were carefully rinsed twice with MilliQ water and oven dried at 40°C overnight. Dried samples were powdered prior to mineralogical analysis through X-Ray Diffraction (XRD). The dried samples were prepared by pipetting ~0.40 mL of an acetone smear containing the precipitate onto a zero-background holder. Samples were then kept in a clean cupboard while the acetone evaporated.

Powder X-ray diffraction was collected from Bruker diffractometers (see Supplementary Material D for details) Rietveld refinements were performed with the software Topas 4.1

(Coelho, 2007). Rietveld quantitative analysis is known to be unreliable for minor phases (<5 wt %) (McCusker et al., 1999). The accuracy is considered to be ± 1-2% for major phases, while the estimated standard deviation from the Rietveld calculation has no bearing on the accuracy or otherwise of the quantification itself, being merely related to the mathematical fit of the model (Madsen and Scarlett 2008). The dried precipitates were also analysed by field emission scanning electron microscopy (FESEM – QEMSCAN 650F FEI) equipped with an energy dispersive X-ray (EDX) detector to examine the morphology (secondary electron) and chemical composition (backscattered secondary electron) of the precipitates. The solid samples were placed on ultra-smooth carbon tape and sputter-coated with submicron layer (~10nm) of gold or carbon prior to SEM analysis.

2.6 *Monohydrocalcite transformation experiment*

To investigate the transformation and stability of monohydrocalcite initially formed in some experiments, we subjected the mineral to elevated temperatures in an aqueous solution. These experiments were designed to investigate what will be the final calcium carbonate polymorph, hypothesizing MHC will transform to more stable phases over time. We recognize that in doing the transformation experiments at elevated temperatures that we have changed the experimental conditions from the lower temperatures of the initial biotic experiments. Approximately 0.02 g of MHC was heated under different media in sealed bottles at 100°C for 48 hours (Munemoto and Fukushi, 2008; Liu et al., 2013). Two milliliters of the following media were used: (1) Atlantic seawater; (2) Mili-Q water; (3) Atlantic seawater with 4.0% w/v yeast extract added; and (4) Atlantic seawater with 750 µM inorganic phosphate (K_2HPO_4 – Molar mass: 174.2 g mol^{-1}). After heating, the media and the solid samples were separated by centrifugation at 4000 rpm for five minutes. The media was decanted and the remaining solids were rinsed with Mili-Q water and dried before analysis by XRD and scanning electron microscope as above.

2.7 *Saturation index and solution chemistry modelling*

PHREEQC (Parkhurst and Appelo, 1999) was used to evaluate the evolution of geochemistry during the experiments. The SIT database (*sit.dat*) was used to model the evolution of the aqueous geochemistry and to calculate the evolution of the saturation indices of the media with respect to relevant calcium carbonate polymorphs (i.e. calcite, vaterite, amorphous

calcium carbonate (ACC) and monohydrocalcite (MHC)). The sit.dat uses the specific ion interaction theory to calculate activity coefficients to calculate saturation state in the media throughout the experiment (Brönsted, 1922; Guggenheim and Turgeon, 1955). The measured concentrations of sulfate and calcium ions were used to predict the evolution of the solution pH and alkalinity of the media at each sampling point. For these predictions we assumed that the decrease in the sulfate concentration was due to microbial sulfate reduction (Gallagher et al. 2012) and that the decrease in calcium concentrations was due to the precipitation of calcium carbonate. The modelled results for the pH and alkalinity were compared to the measured pH and alkalinity titrations to inform on the validity of the model described above. In the case of a large discrepancy between the modelled and measured alkalinity and pH, the alkalinity was adjusted in the model through the addition of $NaHCO_3$ to approximate the (de)sorption of carbonate ions from the kaolinite or calcite surfaces, and the pH was adjusted by the release of CO_2(g) to approximate (partial) equilibration with a low CO_2 headspace. The final results of the model were used to calculate the ion activity product (IAP: log a_{Ca2+} a_{CO32-}) to determine the saturation state with respect to ACC, which is log (IAP/K_{sp}) or log Ω (logK_{sp} = -6.40; Brecevic and Nielsen, 1989), monohydrocalcite (logK_{sp} = -7.60; Hull and Turnbull, 1973), vaterite (logK_{sp} = -7.90; Plummer and Busenberg, 1982), aragonite (logK_{sp} = -8.33; Plummer and Busenberg, 1982) and calcite (logK_{sp} = -8.48; Plummer and Busenberg, 1982).

3.0 RESULTS

3.1 *Evolution of aqueous chemistry*

The results are separated by the seeding material used in each experiment (kaolinite seeds versus calcite seeds). All killed controls and saturation indices for carbonate polymorphs other than MHC are presented in Supplementary Materials E.

3.1.1 *Experiment with kaolinite seeds*

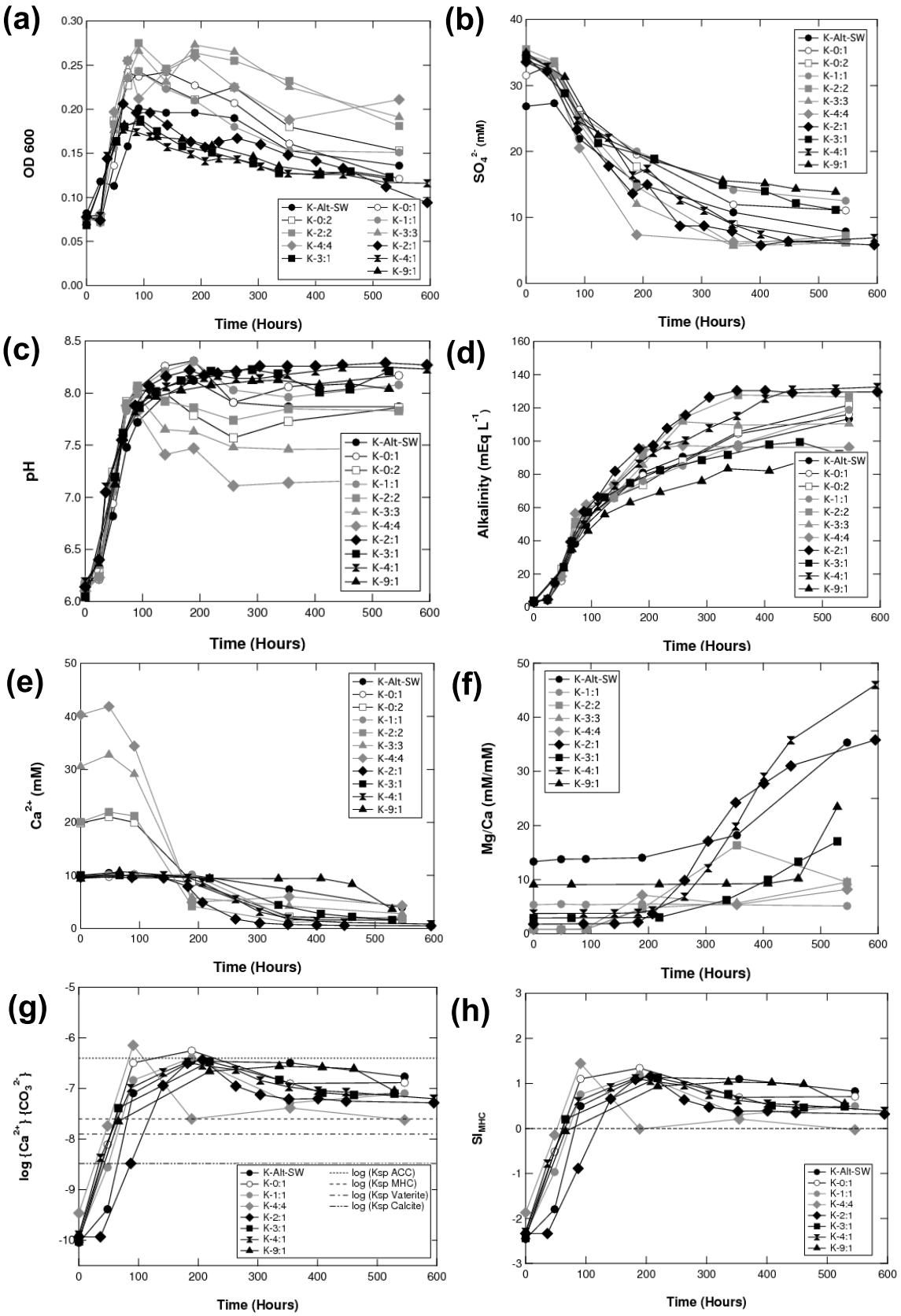

Figure 1: Aqueous chemistry data for the experiments with kaolinite seeds (a) optical density; (b) SO_4^{2-}; (c) pH; (d) total alkalinity; (e) Ca^{2+}; (f) Mg/Ca ratio; (g) ionic activity product for $CaCO_3$;

and (h) SI_{MHC} calculated immediately after inoculation until 546 hours. We did not observe any significant change in the killed samples (shown in supporting online material F). Sample code explanation – K = kaolinite seeded; C = calcite seeded; 3:1 = Mg 30 mM: Ca 10 mM; Alt-SW = Atlantic Seawater (Mg/Ca = 5.2) [See Table 1].

Significant bacterial growth was observed in all incubated samples over the first 100 hours after which the bacteria reach stationary growth phase (OD 600~0.15 – 0.25) (Figure 1a). Bacterial growth is not detected in the killed control samples (see Supplementary Material F). The pH in all incubated samples increases to ~8 as microbial sulfate reduction progresses (Figure 1 b and c). After 100 hours, carbonate mineral precipitation is observed in K-2:2, K-3:3 and K-4:4 (with Mg/Ca of 1 and magnesium and calcium concentrations at 20, 30 and 40mM, respectively). Experiments K-0:1 and K-1:1, with lower calcium concentrations, reach a higher pH before carbonate mineral precipitation starts around 200 hours. A greater magnitude of pH drop (approximately 1 pH unit) is evident in K-4:4 compared to the other vials. Delayed precipitation of calcium carbonate is observed in seawater samples (K-Alt-SW). All experiments began with total alkalinity of approximately 4.0 ± 0.5 mEq L^{-1}, which then increases to greater than 100 mEq L^{-1}. The alkalinity for experiments K-2:2 and K-4:4 plateaus earlier (200 and 250 hours) relative to the other experiments (Figure 1d). The rate of calcium carbonate precipitation, as indicated by the decrease in the calcium concentration, increases with increasing initial calcium concentration (Figure 1e). Sulfate concentrations decrease over time, although they are never fully depleted. We note that the rate of sulfate depletion slows as carbonate minerals begin to precipitate. We observe a dramatic increase in the Mg/Ca ratio over time (Figure 1f). Samples with initial calcium concentration greater than 20 mM experienced a sharp increase in the saturation index or log Ω (saturation state) for all carbonate polymorphs at 100 hours. This increase in saturation index is most dramatic where the kaolinite seeded samples reached (or nearly reached) the K_{sp} of ACC. We observe that nearly double the amount of time is required for samples with 10 mM calcium to reach their highest ionic activity product (IAP) and precipitation starts to slow down or stop when IAP starts to drop (Figure 1g and h).

3.1.2 Experiments with calcite seeds

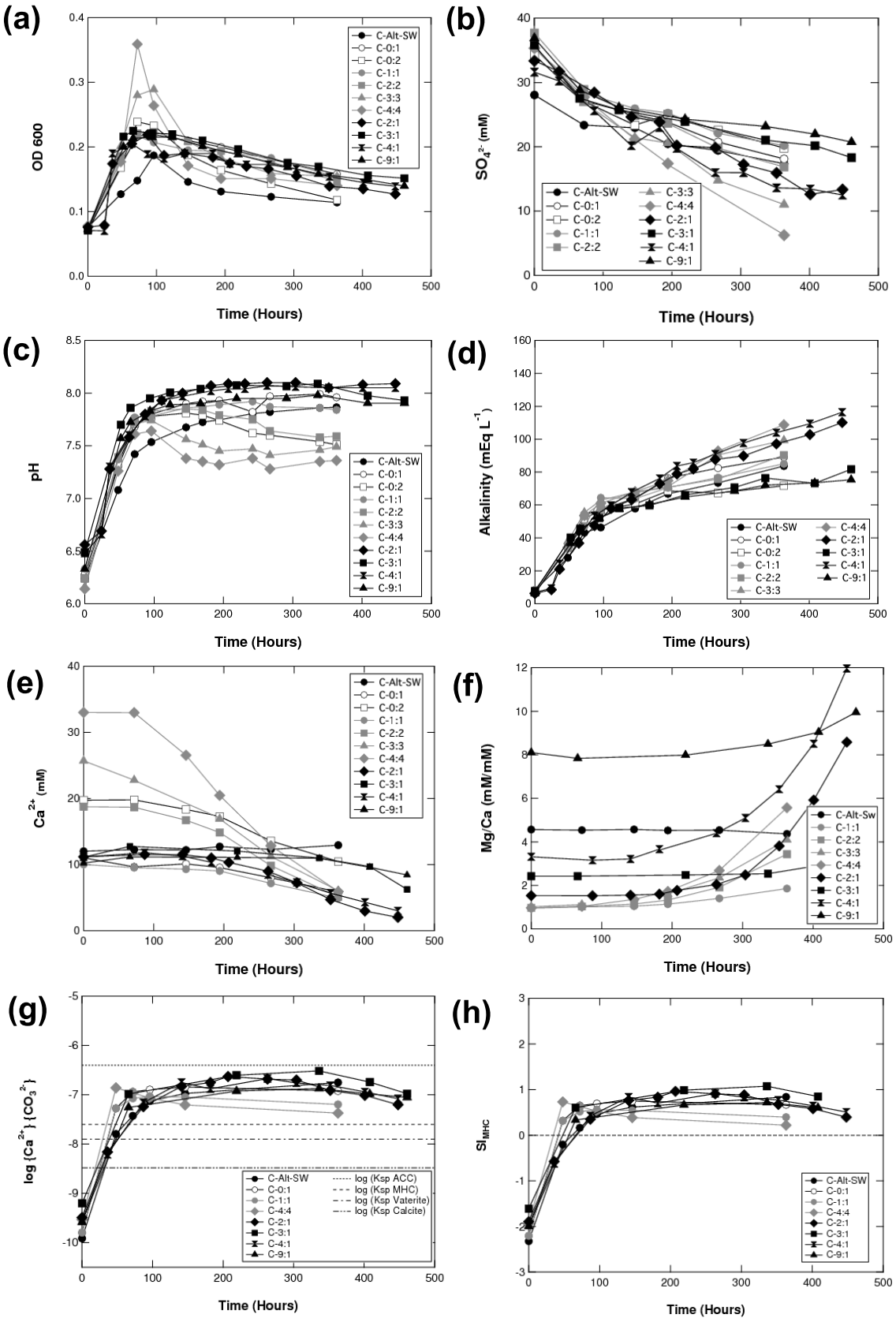

Figure 2: Aqueous chemistry data for the experiments with calcite seeds (a) optical density; (b)

SO_4^{2-}; (c) pH; (d) total alkalinity; (e) Ca^{2+}; (f) Mg/Ca ratio; (g) ionic activity product for $CaCO_3$; and (h) SI_{MHC} measured immediately after inoculation until 546 hours. A drop in pH and calcium concentrations in C-Alt-SW is not apparent although precipitation of MHC (measured by XRD and SEM) occurred. Sample code explanation – K = kaolinite seeded; C = calcite seeded; 3:1 = Mg 30 mM: Ca 10 mM; Alt-SW = Atlantic Seawater (Mg/Ca = 5.2) [See Table 1].

Similar to experiments with kaolinite seeds, we observe a sharp rise in OD 600 and pH linked to microbial sulfate reduction within the first 100 hours (Figure 2a, b and c), which stabilizes and then gradually drops in the samples with Mg/Ca of 1 at higher absolute magnesium and calcium concentrations (C-3:3 and C-4:4). Although the experiment starts at a lower pH of 6.2 – 6.5, the calcite seeds survive the first 50 hours of undersaturation (gravimetric data showing no loss of calcite seeds is presented in Table 6, Supplementary Material F). Total alkalinity increases to maximum values of 110 mEq L^{-1}, compared to the experiments with kaolinite seeds in which alkalinity increases to a maximum of 130 mEq L^{-1}. The concentration of phosphate, which is sourced from the yeast extract, was measured in this experiment (data shown in Supplementary Materials G) and initially ranged from 600 – 850 µM and gradually decreases by 50 to 500 µM as the experiment progresses. We observe a decrease in calcium and sulfate concentration (Figure 2b and e), although at a lower rate than in the experiments with kaolinite seeds, and an increase in the Mg/Ca (Figure 2f). The K_{sp} for ACC in the experiment with calcite seeds is not reached (Figure 2g). The saturation index for the various calcium carbonate polymorphs (MHC, calcite, and aragonite) is lower than the saturation index with kaolinite seeds (Figure 2h and 1h) ($SI_{calcite}$, $SI_{aragonite}$, and $SI_{vaterite}$, are reported in Supplementary Materials E).

3.2 *Results from geochemical modelling*

PHREEQC was used both to calculate the saturation index for various carbonate polymorphs (Figures 1h and 2h) as well as to model the evolution of alkalinity over the experiment. In the alkalinity model, we note a greater discrepancy between the experimental and the modelled alkalinity in the experiments with kaolinite as seeding material (Figure 3a and c) than those with calcite as seeding material (Figure 3b and d). Despite the mismatch in some of the calcite seeding samples (Figure 3d), we are able to model most of the samples with good agreement between the measured and modelled alkalinity.

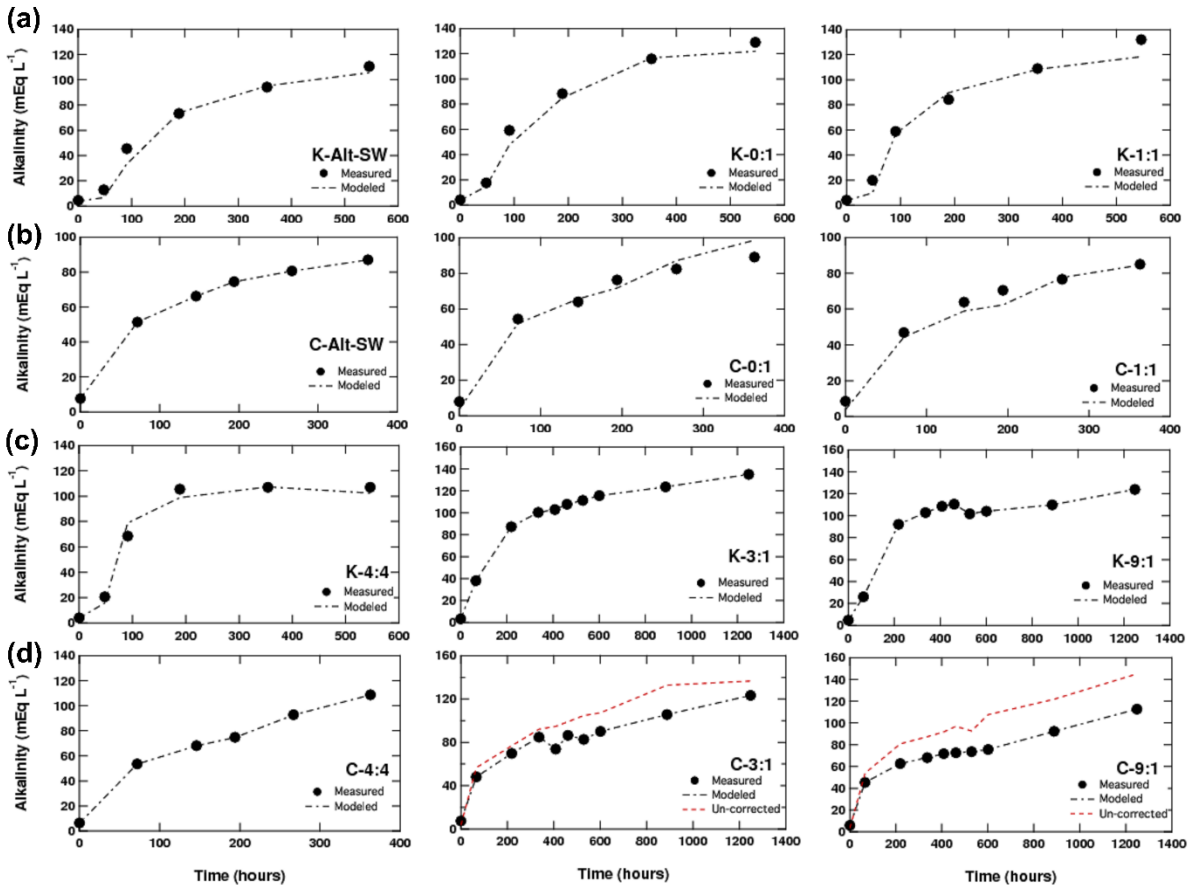

Figure 3: Comparison of experimental and modelled evolution of aqueous chemistry in samples with different seeding materials. A larger discrepancy between experiment and model was observed in samples with kaolinite seeds (a and c) compared to calcite seeds (b and d). An increase in the mismatch between experimental and modelled results is observed with an increasing Mg/Ca. The line labelled 'uncorrected' indicates the initial modelled values without any addition or removal of $NaHCO_3$ from the solution input.

3.3 Results from mineralogical characterization

Table 2: Summary of XRD results with Rietveld quantitative analysis of minerals (wt % with estimated standard deviation) for all experiments. Calcite and Magnesium Calcite differ in their concentration of magnesium and have different XRD patterns.

Experiment – Mg:Ca	Mg/Ca	Kaolinite (wt %)	Calcite (wt %)	Magnesium calcite (wt %)	Monohydrocalcite (wt %)
K-0:1	0	87.4 ± 0.4	12.6 ± 0.4	-	-
C-0:1	0	-	100.0 ± 2.6	-	-
K-0:2	0	72.7 ± 2.9	27.3 ± 1.3	-	-
C-0:2	0	-	100.0 ± 2.0	-	-
K-1:1	1	86.7± 3.4	12.7 ± 1.3	-	-
C-1:1	1	-	87.2 ± 2.2	12.6 ± 1.1	-
K-2:2	1	84.6 ± 1.8	-	15.4 ± 0.7	-
C-2:2	1	-	85.2 ± 1.7	14.8 ± 1.7	-
K-3:3	1	80.5 ± 1.6	-	19.6 ± 0.7	-
C-3:3	1	-	55.6 ± 2.4	44.3 ± 2.2	-
K-4:4	1	66.1 ± 1.6	-	33.8 ± 1.0	-
C-4:4	1	-	44.6 ± 2.7	55.5 ± 3.0	-
K-2:1	2	92.4 ± 1.4	-	2.6 ± 1.2	5.0 ± 0.8
C-2:1	2	-	88.9 ± 2.2	11.1 ± 2.2	-
K-3:1	3	90.3 ± 1.2	-	-	9.7 ± 1.0
C-3:1*	3	-	76.0 ± 2.0	21.0 ± 1.6	3.0 ± 0.6
K-4:1	4	85.5 ± 1.0	-	-	14.5 ± 1.0
C-4:1	4	-	93.4 ± 0.7	-	6.6 ± 0.7
K-Atl-SW	5.2	87.5 ± 1.0	-	-	12.5 ± 1.0
C-Atl-SW	5.2	-	87.7 ± 2.3	4.0 ± 0.8	8.2 ± 0.5
K-9:1	9	87.6 ± 0.9	-	-	9.5 ± 0.8
C-9:1	9	-	86.1 ± 1.1	-	13.9 ± 1.0

* Average of two samples.

Characterization of the solid samples using XRD showed that two calcium carbonate polymorphs precipitated from all experiments: MHC and calcite (Table 2). Our experiments

suggest that all solutions with Mg/Ca ratio of greater than 3 dominantly yield MHC, whereas the media with an initial Mg/Ca of 1 or less produces calcite (Table 2). The diffraction patterns for MHC and calcite align closely with the crystallographic information for $Mg_{0.1}Ca_{0.9}CO_3$ (Althoff, 1977) (Figure 4). The calcite peak becomes broader and shifts towards higher 2θ over time and with increasing magnesium concentration in the medium (Figure 4b). This peak shift and broadening suggests the incorporation of magnesium into the lattice of calcite, decreasing the size of the unit cell and the crystal domains (Lenders et al., 2012; Nielsen et al., 2016; Blue et al., 2017). We observe that the mineralogy of the polymorphs precipitated is weakly affected by the type of seeding material.

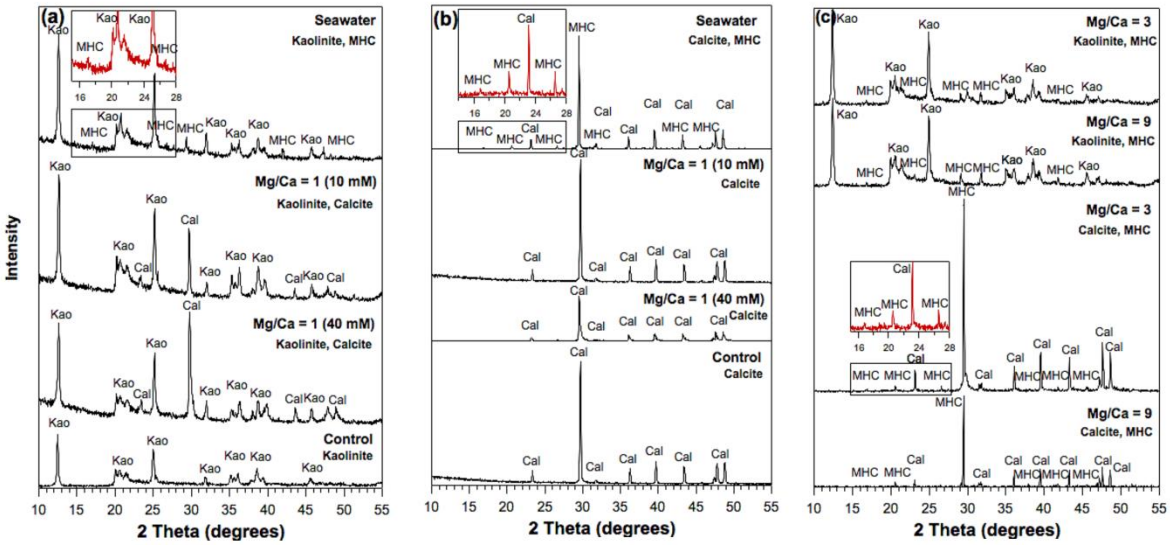

Figure 4: Powder X-Ray diffraction patterns collected from selected incubation samples in the three biotic experiments, (a) Mg/Ca=1 (kaolinite); (b) Mg/Ca=1 (calcite); and (c) Mg/Ca=3 and 9 (kaolinite and calcite). Intensity is reported in counts.

3.4 *Microbial evidence in mineral precipitates*

In the SEM images we observe spherulitic MHC with a hollow core where clumps of well-preserved bacterial cells are located (Figure 5a and b). Duplets or triplets of spherulitic MHC are also common (Figure 5b). In addition to the spherical MHC found, a dumbbell-shaped structure with microbial imprints was also identified in our experiments (Figure 5c). Figure 5d shows the jagged calcite structure (bottom right) is precipitated adjacent to the calcified bacteria colony (upper left). Note the distinct texture of both structures where the calcite is

micrometer in size with unique triangular ends while the bacterial cells are calcified by sub-micron to nano-meter scale crystals.

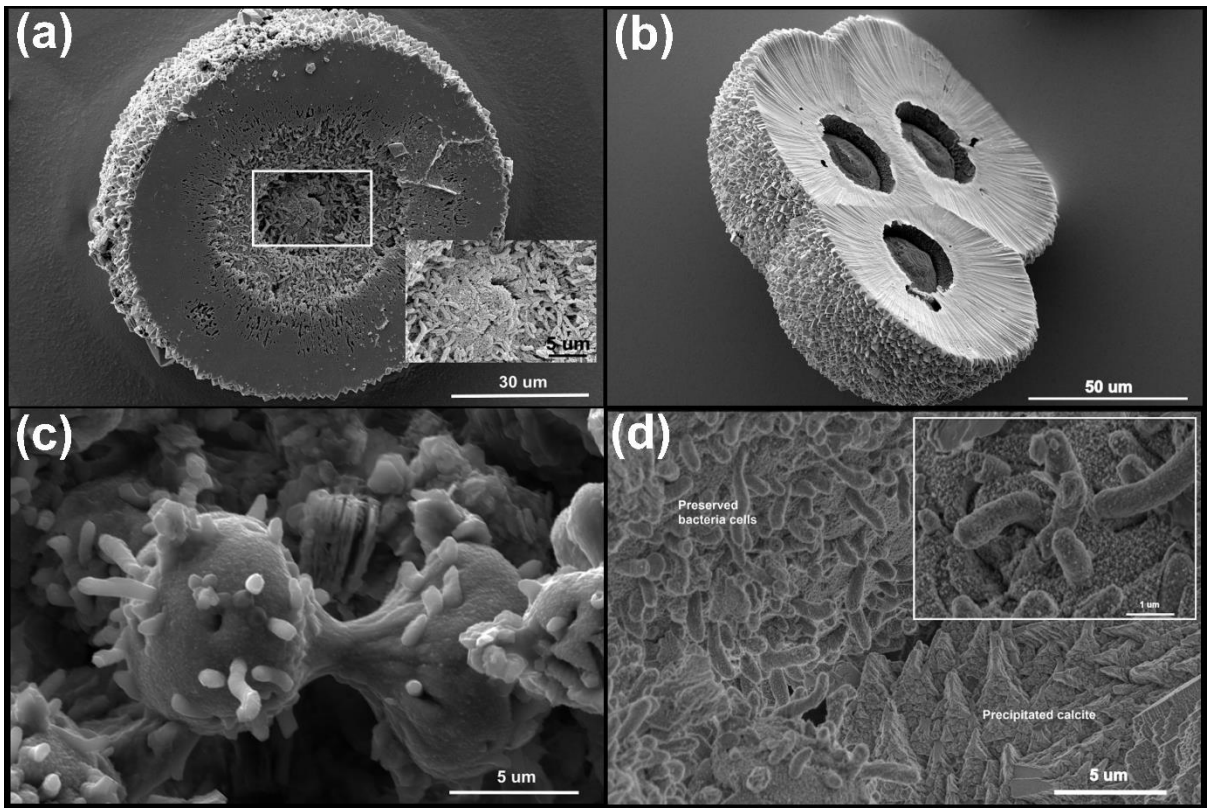

Figure 5: SEM images (backscattered electron) showing (a) MHC hemisphere with bacteria colony concentrated at the hollow core – sample C-Alt-SW; (b) triplet hemi-spherulitic MHC structure with hollow core – sample C-Alt-SW; (c) dumbbell-shaped structure with protruding well-preserved bacterial cell observed in sample K-4:4; (d) precipitated calcite located adjacent to fossilized bacterial colony – sample K-4:4 with closeup secondary electron (SE) image showing instantaneous calcification of Desulfovibrio bizertensis by the nano-sized crystals. All the images showing the morphology and microstructure of carbonate minerals linked to microbial sulfate reduction.

3.5 *Transformation experiment*

Four different media combinations were tested to examine which stable calcium carbonate polymorphs form from the MHC produced during our experiments (Table 3). For this, pure, spherulitic MHC is used (with diameter range between 20 – 40 µm) which had been previously precipitated from an unseeded incubation (Figure 6a). Here, we also show abiotically

precipitated MHC for comparison purpose (Figure 6b). There is a distinct size and morphological difference between the biotic and abiotically precipitated MHC (Figure 6a and b). In pure seawater, this MHC transforms into both calcite and aragonite (Table 3). In this case, the dehydration of MHC changes its spherulitic structure to elongated needle-like calcite and aragonite crystals (Figure 6c). Incubation of MHC with pure MQ-water transforms the MHC into calcite (Figure 6d). In contrast, when the transformation happens in seawater with yeast extract or inorganic phosphate, a considerable amount of MHC is retained and not transformed into a more stable calcium carbonate polymorph (sample T-Alt-SW-YE - 79.5 ± 1.5 %, sample T-Alt-SW-PO4 - 26.2 ± 1.7%) (Figure 6e and f).

Table 3: Mineralogical composition of calcium carbonate polymorphs (in wt %) derived from MHC transformation.

Medium	**MHC**	**Calcite**	**Mg-Calcite**	**Aragonite**
T-Atl-SW (Seawater only)	-	77.1 ± 3.9	-	22.9 ± 3.9
T-MQ (MQ-water only)	-	100.0 ± 0	-	-
T-Atl-SW-YE (Seawater + yeast extract)	79.5 ± 1.5	15.5 ± 1.2	5.1 ± 1.2	-
T-Atl-SW-PO4 (Seawater + K_2HPO_4)	26.2 ± 1.7	52.3 ± 3.1	-	17.2 ± 1.3

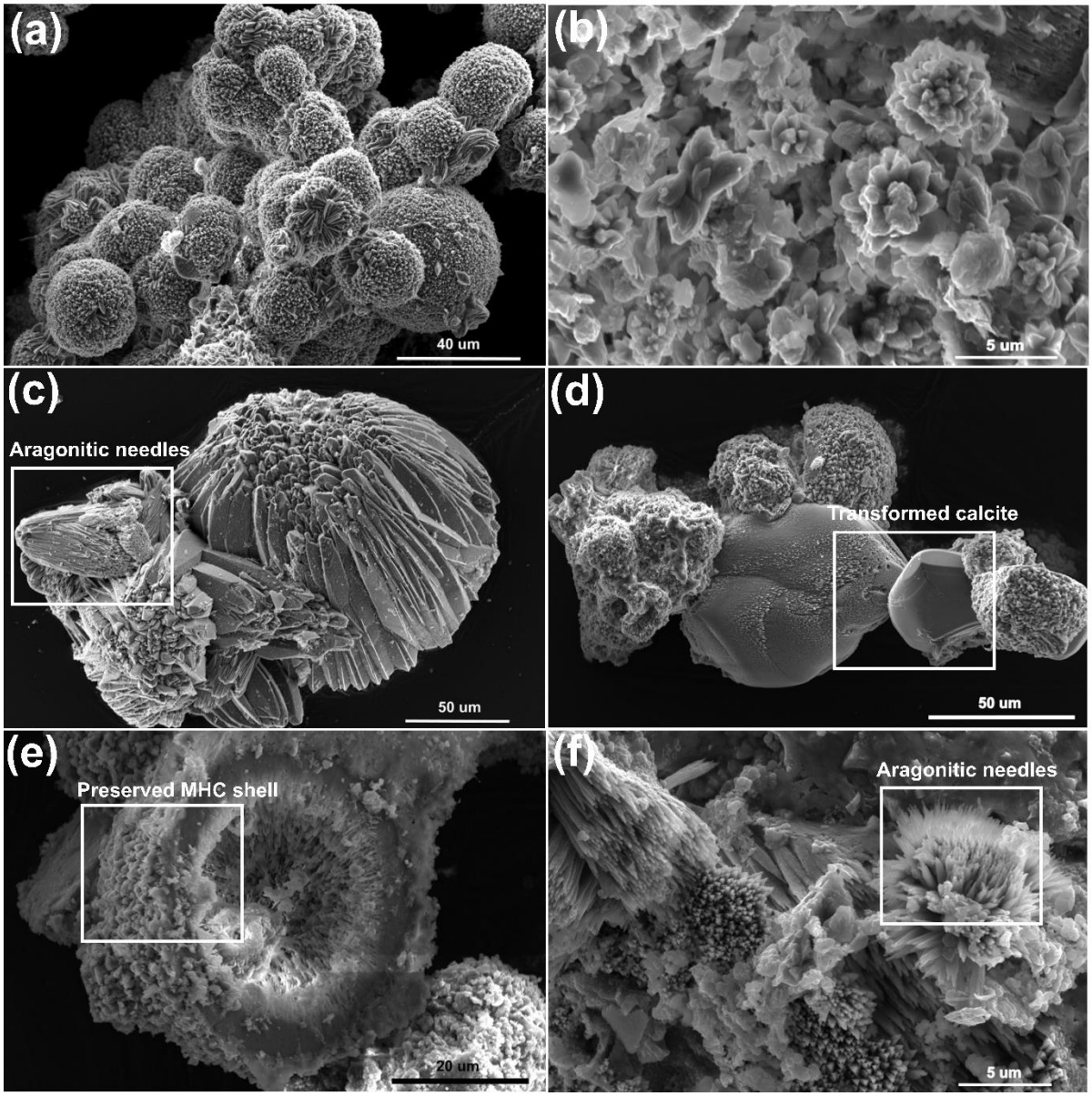

Figure 6: SEM images show the morphology of minerals precipitated in the biotic and abiotic experiments. (a) Initial spherulitic MHC from the biotic experiments; and (b) sub-micron aggregated platelets (cauliflower-shaped) MHC from abiotic experiment. The mineralogy of these final products was confirmed using XRD. Image (c) – T-Alt-SW, (d) – T-MQ, (e) – T-Alt-SW-YE, and (f) – T-Alt-SW-PO4 are transformation products of 5a after thermal dehydration at 100˚C for 48 hours. We note the distinct morphological alteration of the final products (aragonitic needles, calcite rhomb and bigger hollow core of preserved spherulitic MHC). Mineral composition of these final polymorphs is reported in Table 3.

4.0 DISCUSSION

Our results indicate that microbial sulfate reduction triggers the precipitation of calcite and MHC. Which of these may dominate appears to depend on the Mg/Ca ratio at the time of mineral nucleation; MHC forms from solutions with Mg/Ca greater than 3, while calcite forms from solution where the Mg/Ca ratio is 1 or less. Our media is initially undersaturated with respect to all carbonate minerals, but within 100 hours the media is super saturated and precipitation of calcium carbonate occurs. The rate of precipitation depends on the calcium concentration in the media, and ironically the mineral seed present, and is independent of the Mg/Ca ratio.

The discussion is divided into five parts. First, we discuss the influence of microbial sulfate reduction on the evolving solution chemistry driving carbonate mineral precipitation. Then we discuss the primary controls on the formation of MHC and calcite in these experiments. Next, we demonstrate the effect of seeding materials on the solution chemistry and also the calcium carbonate polymorphs precipitated. In the penultimate section of the discussion, we show the controls on the transformation of MHC to more stable polymorphs. Finally, we explore the implications of our results on sedimentary carbonate precipitation in the natural environment.

4.1 The influence of microbial sulfate reduction on calcium carbonate precipitation

Our experimental results show that microbial sulfate reduction strongly influences solution chemistry and thus, affects carbonate mineral precipitation in three ways. First, each experiment is accompanied by a significant increase in total alkalinity and pH as microbial sulfate reduction proceeds (Figures 1d, 2d) through the overall reaction (Gallagher, 2012):

$$4CHO_2^- + SO_4^{2-} + H_2O \rightarrow 4HCO_3^- + HS^- + OH^- \quad \text{(Eq. 1)}$$

This relationship suggests an increase of one mole of dissolved inorganic carbon (DIC) as well as an increase of 1.2 moles of total alkalinity per mole of organic carbon oxidized (Soetaert et al. 2007). This increase in alkalinity leads to dramatic increases in the carbonate mineral saturation state. For example, within the first 100 hours of experiments with kaolinite seeds, we see a 10 to 15-fold increase in alkalinity, which translates to calcite saturation index of ~1 - 2 ($SI_{Calcite}$). After carbonate mineral growth begins, the continued increase in pH and DIC

456 from the growth of the sulfate reducing bacteria is matched by a decrease or stabilization of
457 the pH and DIC concentration due to calcium carbonate precipitation.
458
459 This increase in alkalinity from microbial sulfate reduction coupled to formate oxidation was
460 closely replicated with PHREEQC modeling for the experiments with the kaolinite seeds, but
461 there was more of a mismatch with the calcite seeds (Figure 3). This suggests that there is a
462 sink for alkalinity in the experiments with calcite seeds that does not exist with the kaolinite
463 seeds. One possibility is the secretion of exopolymeric substances (EPS) by the sulfate
464 reducing bacteria, which can complex cations across a wide range of solution pH (Braissant et
465 al., 2007; Dupraz et al., 2009; Baker et al., 2010). EPS was not included in the PHREEQC model,
466 nor was the concentration or type of EPS analysed during the experiment. Another possibility
467 is that the adsorption onto and desorption from the mineral seeds' surfaces, and the
468 exchange of CO_2 with the headspace might account for alkalinity difference in the model.
469 Despite the mismatch in some of the calcite seeding samples, we were able to model most of
470 the samples with good agreement between the measured and modelled alkalinity (figure 3).
471
472 Although Soetaert et al. (2007) suggested that microbial sulfate reduction alone may not lead
473 to carbonate mineral precipitation because the solution pH is poised too low (the equivalence
474 midpoint is pH 6.7), recent modelling and culture experiments support the notion that
475 microbial sulfate reduction may lead to carbonate mineral precipitation. For example, Meister
476 et al. (2013) demonstrated that while microbial sulfate reduction initially lowers pH, the
477 carbonate saturation state decreases at first but slowly increases as sulfate reduction
478 continues due to increasing dissolved inorganic carbon concentration while pH stabilizes. The
479 Meister et al (2013) results are in agreement with our observations – that the chemical
480 evolution of closed (or diffusionally controlled) systems is strongly dependent on the amount
481 of organic carbon respired, and therefore dissolved inorganic carbon generated, in addition
482 to other variables such as pH and buffering capacity.
483
484 Second, aside from increases in dissolved inorganic carbon and carbonate saturation state,
485 the concentration of inhibitors of carbonate mineral precipitation, such as sulfate and
486 magnesium, changes over the course of our experiments (Walter and Burton, 1986; Burton
487 and Walter, 1989; Grases and March, 1990; Lin and Singer, 2005). Although sulfate has long

been understood to inhibit calcite precipitation (Busenberg and Plummer, 1985; Walter, 1986 Bots et al., 2011), especially in the presence of elevated concentrations of aqueous magnesium (Bots et al., 2011; Nielsen et al., 2016; Dobberschutz et al., 2018), our results show that calcium carbonate mineral nucleation occurs as sulfate is being depleted, but while there is still substantial aqueous sulfate in solution. Furthermore, the Mg/Ca ratio in our solution increases over the course of the experiments. Because the Mg/Ca ratio is recognized as a fundamental control on calcium carbonate polymorphism, changes in this parameter should influence the final carbonate mineral products.

Together, solution data from our experiments show that microbial sulfate reduction alters the chemical state of the experiments with respect to calcium carbonate mineral stability. The sulfate reducing bacteria, through their metabolism, produce an extremely high saturation state for all calcium carbonate polymorphs, which triggers nucleation in the presence of multiple inhibitors to nucleation and growth. The SEM images (Figure 5) of the carbonate minerals precipitated suggest that the sulfate reducing bacteria create a highly supersaturated micro-environment driving carbonate precipitation. We suspect that the negatively charged cell surface of the sulfate reducing bacteria initially attracts dissolved divalent cations such as calcium and magnesium (Qiu et al., 2017). During carbonate precipitation, outward growth of crystals from a substrate eventually introduces geometrical competition where crystals growing normal to the substrate dominate over other orientations; this typically results in outward radiating crystal fabrics which may sometimes adopt a spherical structure if they are grown on a rounded or spherical substrate (i.e., aggregate of bacterial cells) (Dickson, 1993). Analogous observations of fossilized bacterial clump in the core of spherulitic carbonates have also been reported from field samples in Chafetz et al., (2018).

It is interesting to note that the spherulitic structure of carbonate minerals is not unique to microbial sulfate reduction. Rather, variables such as Mg/Ca ratio (between 2 to 8), salinity, nucleation surfaces, and precipitation rates collectively control the habit and structural form of the carbonate precipitated (Tracy et al., 1998; Sanchez-Navas et al., 2009; Nyiro-Kosa et al., 2018). Spherulitic growth is also a common product resulting from crystallization of ACC. Spherulitic growth requires a large crystallization driving force, such as a solution with

sustained supersaturation from initial formation and subsequent continuous dissolution of ACC, resulting in the aggregation and growth of spherical nanoscale mineral particles (Granasy et al., 2005; Han et al., 2017a; Rodriguez-Blanco et al., 2017). Some field sedimentary characteristics of dolomite also reflect spherulitic growth processes, suggesting that the deposition and crystallization process may have involved the transformation of an amorphous precursor, and thus high supersaturation states (Hood et al., 2011). The hollow core structure of the spherulitic MHC with calcified microbes texture in our experiments are not visible in the carbonate precipitation products during abiotic precipitation experiments (Bots et al., 2012; Rodriguez-Blanco et al., 2014), hence, could serve as unique signature of microbially-mediated precipitation. However, our transformation experiments suggest that such a structure and the associated microbial texture are difficult to preserve when stable carbonate polymorphs are formed and thus could be vulnerable to post-burial processes during early diagenesis.

We suspect our carbonate mineral products must have initially transformed from an amorphous phase (ACC) prior to crystallization into calcite or MHC. The amorphous phase is often found present together with some other crystalline sample with Bragg peaks on the XRD pattern. Visual examination under SEM also indicates that both amorphous and crystalline solid phase coexist during the early stage of the precipitation (Supplementary Materials H). Furthermore, as we discuss below, saturation state and calcium carbonate mineralogy provide additional evidence for the role of an amorphous calcium carbonate precursor. Depending on the Mg/Ca ratio of the surrounding fluid, the ACC and calcite may incorporate different amounts of water into the structure due to the difference in hydration energy between the magnesium and calcium ions (Christ and Hostetle, 1970; Gonzalez, 2009; Tommaso and de Leeuw, 2010; Hopkinson et al., 2012; de Choudens-Sanchez and Xu et al., 2013; Nishiyama et al., 2013; Sun et al., 2015). Such a difference in hydration energy has also been shown to affect the transformation into crystalline calcium carbonate polymorphs and induce the transformation of ACC to MHC rather than calcite (Rodriguez-Blanco et al., 2014). The structure of calcite precipitated in the experiments with lower Mg/Ca forms rhombohedral shapes with triangular terminations (Figure 6d).

4.2 Evolving chemical controls on $CaCO_3$ precipitation and polymorph selection

552 The chemical evolution discussed above establishes a framework for interpreting the mineral
553 products formed in our experiments, and for predicting the calcium carbonate mineral phases
554 that may be associated with microbial sulfate reduction more broadly in the natural
555 environment. An unexpected observation from our experiments is the dominance of MHC in
556 the biomineralization products, a relatively rare calcium carbonate polymorph in natural
557 systems. Previous work suggests that at Mg/Ca ratios of greater than ~2, aragonite nucleation
558 dominates calcium carbonate mineral precipitation, and therefore the carbonate mineral
559 products precipitated from modern seawater (Katz, 1973; Berner, 1975; Burton, 1993, Ries et
560 al., 2008; Bots et al., 2011). However, aragonite is conspicuously absent in all of our
561 experiments (and, indeed, in nearly all microbially induced carbonate precipitation
562 experiments) despite initial Mg/Ca ratios that ranged from 0 – 9 (Table 2). This hints at a
563 strong inhibition of aragonite nucleation in our experiments, remembering that aragonite has
564 a higher energy barrier to nucleation compared to other polymorphs such as MHC, which we
565 suspect results from elevated phosphate concentrations. Previous studies have shown that a
566 phosphate concentration of greater than 10 μM inhibits the formation of aragonite, and even
567 phosphate concentrations as low as 5 μM can alter the kinetics of aragonite precipitation
568 (Walter, 1986; Oomori et al., 1988; Burton and Walter, 1990; Yagi and Fukushi, 2011; Tadier
569 et al., 2017). The phosphate concentration in our experiments ranged between 600 – 800 μM,
570 which is on the higher range of that measured in anoxic sediments (Sasaki et al., 2001;
571 Hyacinthe and Van Cappellen, 2004; Sinkko et al., 2013; Egger et al., 2015; Kipp and Stueken,
572 2017). We suspect that the high range of phosphate concentrations in our experiments
573 inhibits the formation of aragonite. In our MHC transformation experiments, the role of
574 phosphate in the inhibition of aragonite is also shown as none of the experiments with added
575 phosphate produced aragonite, in spite of high Mg/Ca; we also observed this in abiotic
576 experiments that we include in Supplementary Materials C. Phosphate adsorbs rapidly and
577 irreversibly on high energy sites (kink, step, edge and hole) of mineral surfaces, which drives
578 the inhibitory effects on carbonate mineral growth and dissolution rates (Berner and Morse,
579 1974).
580
581 One possible consequence of the presence of phosphate in our experiments is that the
582 saturation state for various calcium carbonate polymorphs increases well beyond typical
583 range needed for aragonite or calcite nucleation from seawater (Morse and He, 1993). In our

584 experiments, we do not observe calcium carbonate nucleation until the ionic activity product
585 is well above that required for initial ACC precipitation (Figures 1g). These solution data hint
586 that, in the absence of aragonite and calcite nucleation, ACC is the solubility-limiting phase in
587 our experiments, providing a reactive and transient precursor to the formation of more stable
588 crystalline calcium carbonate mineral phases.
589
590 In addition to the exceptionally high saturation states needed for carbonate mineral
591 precipitation, the likely initial formation of ACC in our experiments provides a simple
592 mechanism to explain observed carbonate polymorphism. Previous studies have shown that
593 once formed, ACC transforms to several carbonate polymorphs depending on the Mg/Ca, pH,
594 and concentration of DIC (Loste et al., 2003; Kimura and Koga, 2011, Nishiyama et al., 2013;
595 Rodriguez-Blanco et al., 2014; Blue et al., 2017). In particular, at high Mg/Ca (above 8,
596 depending weakly on pH and concentration of dissolved inorganic carbon) ACC has been
597 shown to transform to MHC.
598
599 Our results suggest that microbial induced ACC transforms to MHC at much lower Mg/Ca than
600 previously shown in these abiotic experiments (Rodriguez-Blanco et al., 2014; Blue et al.,
601 2017). Our results, for the timepoint of precipitation, are superimposed on the stability fields
602 for MHC initially proposed by Blue et al. (2017) (Figure 7). We show that dominant carbonate
603 mineral polymorph is determined by the solution chemistry at the time of carbonate mineral
604 nucleation, and although the solution chemistry then evolves into other stability fields
605 (Supplementary Material I), the initially precipitated polymorph continues to grow. Our
606 experiments suggest a shift in the calcite-MHC boundary to a $a\mathrm{Mg}^{2+}/a\mathrm{Ca}^{2+}$ of 2. However, the
607 abiotic experiment in Blue et al. (2017) did not have phosphate which we already suspect has
608 influenced carbonate mineralization pathways. Therefore, the apparent stability field
609 suggested by this study may be partly due to the role of phosphate.
610
611 These experimental results suggest that the experiments where MHC precipitates (higher
612 Mg/Ca ratios) have a longer delay prior to initial mineral precipitation, and a lower pH drop
613 compared to the experiments that precipitate calcite. This may be due to the incorporation
614 of magnesium in the initial ACC, which has been suggested to stabilize ACC and retard the
615 time required for transformation (Lin et al., 2015; Purgstaller et al., 2017). In addition,

magnesium incorporation likely decreases the effective solubility of both the ACC and MHC polymorphs, although this is not quantitatively understood at present (Fukushi et al., 2017; Purgstaller et al., 2017).

The evolution of solution chemistry and the formation of different calcium carbonate polymorphs here are comparable to other experiments involving carbonate mineral precipitation and microbial populations conducted by Balci et al. (2016) and Han et al. (2017). Both studies investigated the role of halophilic bacteria in the precipitation of carbonate minerals. Dypingite, hydromagnesite, aragonite, MHC, huntite and struvite were the primary carbonate minerals that precipitated from a hypersaline solution (Balci et al., 2016; Arias et al., 2017) whereas Han et al., (2017) found MHC, calcite and Mg-rich calcite in varying sodium chloride solutions (3 – 20% w/v) cultured with *Chromohalobacter Israelensis*. In contrast to culture experiments reported by Rivadaneyra et al., (1998; 2010), our culture samples with high (Mg/Ca = 3) did not precipitate any aragonite. This is probably due to the fact that Rivadaneyra et al., (1998; 2010) incubated their samples at a higher temperature (32˚C) and liquid-limited environment (a glass coverslip) – however the presence of water molecules (or activity of water) is the key for hydrated phase MHC to form.

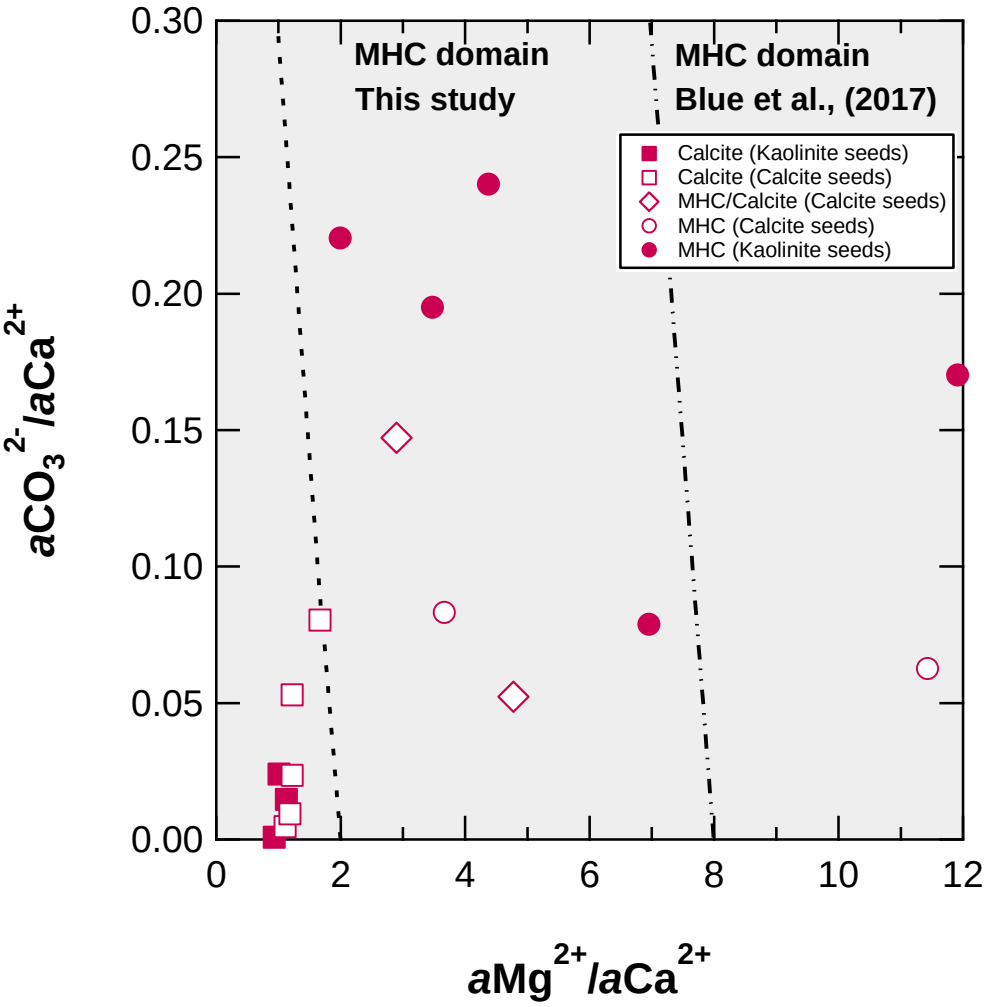

Figure 7: The stability field for MHC and calcite. *The data points are taken from the point in the experiment where precipitation occurs, although the initial solution chemistry and subsequent solution chemistry evolve (for plots with this evolution see Supplementary Material I). Square symbols indicate calcite is the final polymorph, circle symbols indicate MHC and diamond symbols have mix mineralogy (both MHC and Mg-calcite). Open symbols mark samples with calcite as seeding material while close symbols are kaolinite seeded samples. Experiments from this study are plotted on an abiotic stability field delineated by Blue et al., (2017) – the dot-dash line. The MHC domain in our experiments (dashed line) has shifted left (from aMg^{2+}/aCa^{2+} approximately 8 to 2).*

In addition to promoting non-traditional calcium carbonate mineralisation pathways in our experiments, high phosphate concentrations might also explain the exceptional stability of MHC in our incubation and transformation experiments. In a phosphate-free solution, any MHC we formed through microbial induction should have transformed into a more stable

carbonate polymorph over time, even at room temperature. However, the precipitated MHC in our experiments did not transform after sitting in the lab over a year with the old media, suggesting something inhibits MHC transformation (Supplementary Material J). Furthermore, the mass basis sorption capacity of MHC is significantly higher than those of aragonite and calcite, which may explain the greater impact of phosphate in stabilizing MHC (Yagi and Fukushi, 2011; Fukushi et al., 2011). It is also possible that the formation of stable calcite/calcium phosphate around the outer shell of the growing crystal shields the inner MHC from transforming by protecting the interior of the spherulitic MHC from exposure to the medium. Besides the role of phosphate in MHC stabilization, previous studies have also suggested the possible role of organic acids such as carboxylic acids and EPS in stabilizing precipitated minerals, where it is thought that the EPS could adsorb or to be entrained within the mineral and significantly reduce its reactivity (Omoike and Chorover, 2006; Steiner et al., 2010; Gallagher et al., 2013).

4.3 Influence of seeding material on the formation of calcium carbonate polymorphs

Microbially-induced carbonate mineral precipitation and polymorphism also appears to depend on the mineral seeds that are present. Overall, MHC tends to dominate products from experiments with kaolinite seeds compared to those with calcite seeds (Table 2 and Figure 8). In addition, MHC forms at slightly lower Mg/Ca ratios in the experiments with kaolinite seeds compared to calcite seeds. We suspect that the delayed and muted precipitation of MHC in calcite-seeded experiments results from initial overgrowth of a higher-magnesium calcite phase on the calcite seeds. Growth of calcite on calcite seeds require a lower supersaturation for nucleation and growth to initiate, thereby lowering the induction time and pH for nucleation to happen. A similar observation has been reported in Lioliou et al. (2007) showing that the types of seeding materials can impact precipitation kinetics. SEM images illustrate an epitaxial growth relationship between the original calcite seeds and precipitated calcite, which ranges from submicron to nano-sized (Figure 9). A similar observation was also reported in Rodriguez-Navarro et al. (2012) where they found that there is an overruling factor of substrate types on the mineralogy of calcium carbonate precipitated. In these experiments, where calcite overgrowth forms, MHC is never observed, and conversely, where there is no calcite overgrowth, MHC precipitates. There are two exceptions to this: the C-3:1 and C-Alt-SW experiments generate products of mixed

mineralogy which could result from multiple precipitation events over the course of the experiment as the Mg/Ca ratio is evolving. No apparent drops in pH or alkalinity were observed in the samples with overgrowth on calcite seeds, suggesting the buffering effects from the calcite seeds impedes high pH values (particularly CO_3^{2-}/Ca^{2+}) in the system, and therefore, MHC is not favoured. Such a difference in precipitation kinetics in experiments with different seeding materials is illustrated in the change of calcium concentration. Nearly all experiments with calcite seeds (except the experiments where we get mixed mineralogy in the final solid products) showed a gradual decrease of calcium concentration while the calcium concentrations drop rapidly in experiments where kaolinite is used. Particularly in the calcite-seeded experiment, we note a trivial drop in calcium concentration prior to the main precipitation event, suggesting slight removal of calcium during the nucleation process (or epitaxial growth on calcite seeds) before main mineral precipitation follows. Homogeneous precipitation is more likely to occur in the kaolinite-seeded experiments where there is less buffering capacity in the supersaturated solution. Such a sample is often characterized by a sharp drop in pH and calcium concentration (e.g. K-9:1).

Intriguingly, these results suggest that MHC is only present at Mg/Ca ratio of 3 in the calcite-seeded experiments; while MHC is dominant at Mg/Ca ratio of 2 in the kaolinite-seeded experiments (Figure 8). Calcite seeds show an increase in the amount of MHC precipitated as the Mg/Ca ratio increases, whereas the amount of MHC precipitated peaks at Mg/Ca = 4 and drop at Mg/Ca > 4 in experiments with kaolinite seeds. We also note that there is less consistency in the carbonate mineral polymorphs precipitated between replicates of calcite-seeded experiments. Such ambiguity is not observed in kaolinite seeded experiment, where the boundary of calcite/MHC domain is more clearly defined at a Mg/Ca ratio of 2.

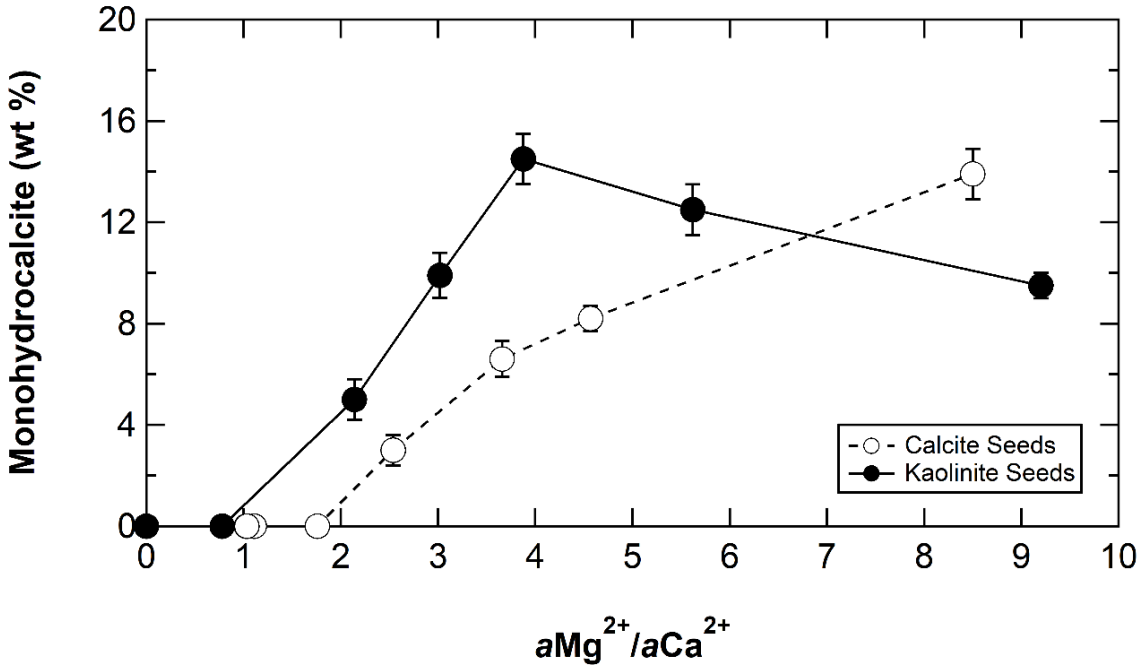

Figure 8: The precipitation of MHC in wt % (of total solid sample) as a function of Mg/Ca (before precipitation) in experiment with different seeding materials. Error bars represent the estimated standard deviation calculated from Rietveld refinement.

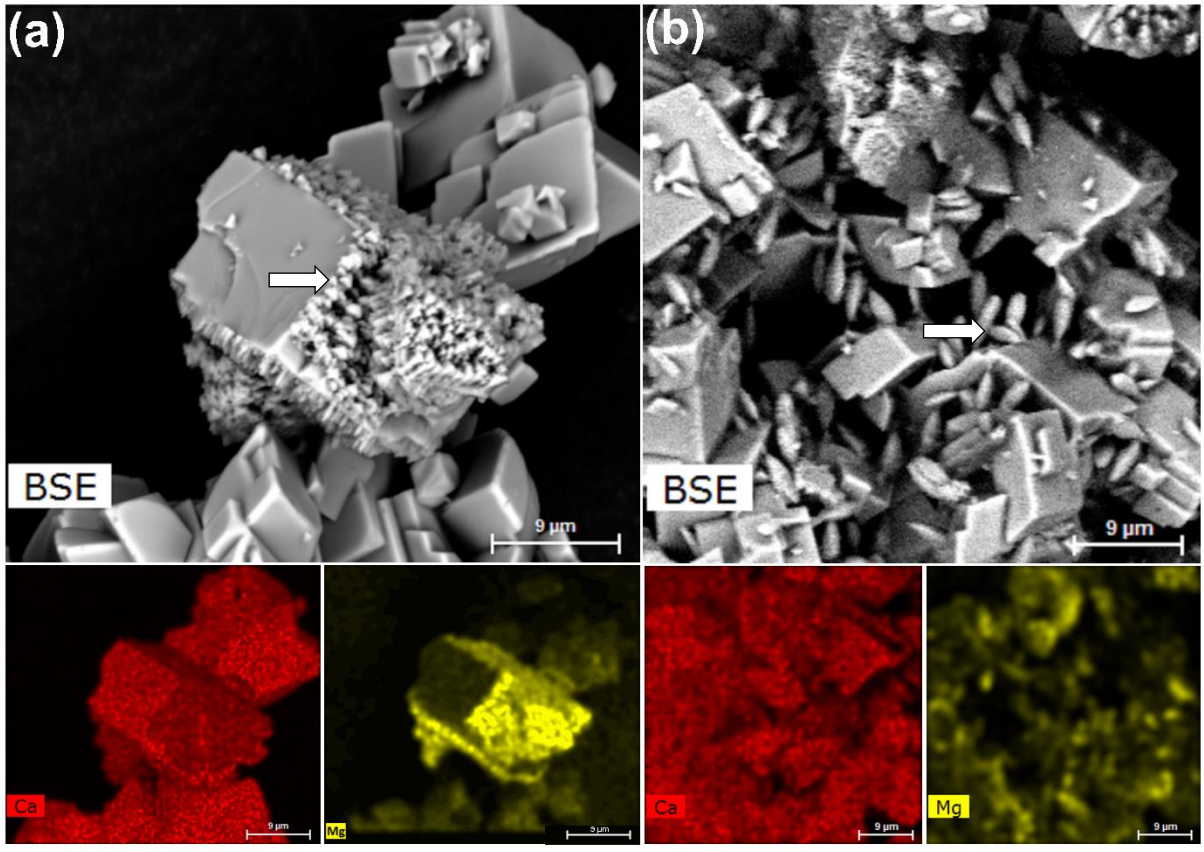

Figure 9: Submicron to nano-sized magnesium calcite crystals grow on calcite seeds (a) C-3:1

and; (b) C-2:1. Arrows show two forms of magnesium calcite growing epitaxially on calcite seeds.

4.4 Synthesis, stability and transformation of MHC

The earliest studies of MHC formation suggest that three conditions had to be met for MHC to form: (1) the Mg/Ca ratio must be high; (2) the water temperature should be < 40 ˚C; (3) The water should be oversaturated with respect to calcite, aragonite, and MHC, while preventing oversaturation with respect to hydroxy- and fluorapatite (Stoffers and Fischbeck, 1974; Oomori et al., 1988). Our results are consistent with these geochemical conditions. Regardless of the seeding material used, we found that SI_{MHC} has to be greater than one for MHC to form (Figure 10). Mixed mineralogy of MHC and calcite (often higher in MHC) is particularly observed at a lower Mg/Ca ratio (between 2 to 4), whereas we found that only MHC precipitate as the Mg/Ca increases. Our results also agree with findings reported by Rodriguez-Blanco et al. (2014) in a series of abiotic experiments where MHC is absence at Mg/Ca lower than two although the solution is highly supersaturated with respect to MHC (SI_{MHC} = 2). However, in their experiments, MHC precipitates when the solution SI_{MHC} approached 2.5 or higher, suggesting that the supersaturated solution alters the precipitation kinetics to favor the formation of MHC. Such a highly saturated condition, however, rarely occurs in biotic studies or in the natural environment.

Contrary to previous work that suggests that it is magnesium that stabilizes MHC, we suggest that phosphate plays a larger role based on abiotic experiments (Supplementary Materials C) and electron backscatter mapping of our samples (Figure 10a and b) (Dejehet et al., 1999). These images indicate that the outer shell of MHC before (Figure 11a and b) and after (Figure 11c and d) the mineralogical transformation is relatively low in magnesium but enriched with phosphorus (Figure 11a, b, c and d). One possible explanation for the stabilization of MHC during the transformation experiment (both T-Alt-SW-YE and T-Alt-SW-PO4) could be the common ion effect, where the solubility of MHC with phosphate absorbed on it decreases. Higher magnesium concentrations were found in the inner shell, suggesting the inner shell is initially composed of more Mg-rich carbonate phases (Figure 11b and c). We suspect that the inner shell could be unstable, nano-crystalline, less dense and associated with the bacterial colony that formed early in the nucleation stage (Supplementary Materials K). The EDS images

743 thus imply the important role of magnesium in MHC nucleation, while phosphate is linked to
744 MHC stabilization. During the transformation process this unstable phase is susceptible to
745 dehydration and deformation via nano-voids or cracks in the MHC, leaving a hollow chamber
746 behind. Comparable features have been previously observed in studies involving other
747 calcium carbonate polymorphs (Suzuki et al., 2006; Chen et al., 2008). Through our
748 transformation experiment, we observe that the phosphate-rich outer layer of MHC is more
749 stable compared to the inner core (Figure 11c), although the exact mechanism how
750 phosphate stabilizes MHC requires further investigation.

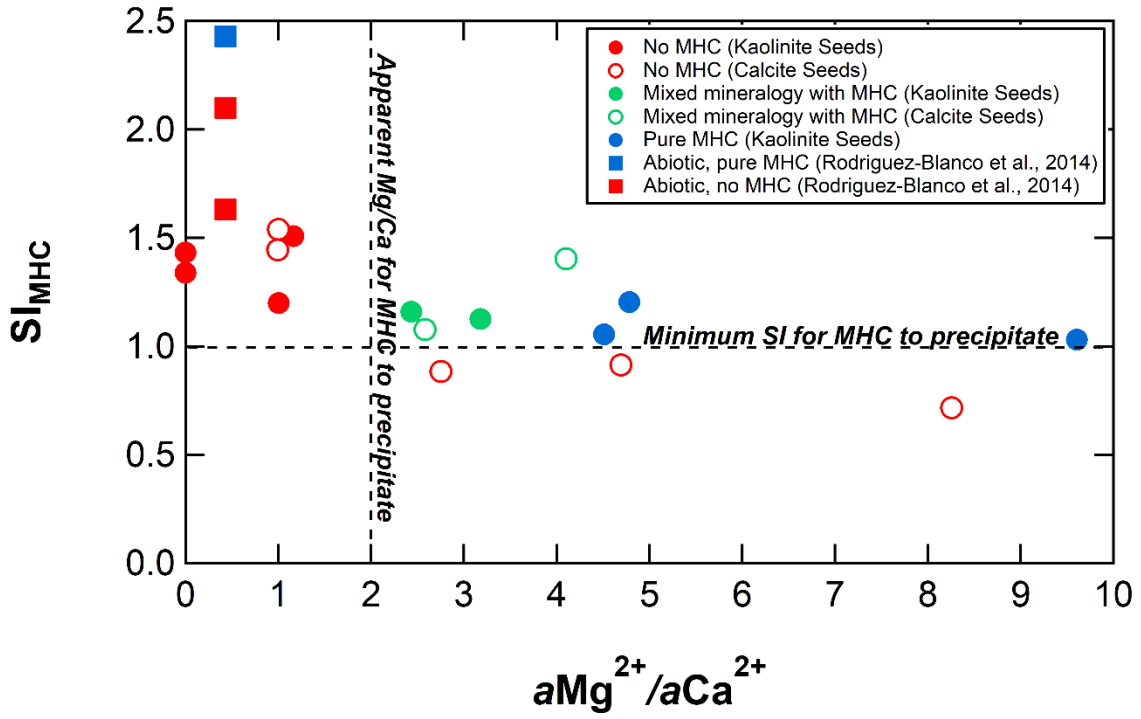

751

752 *Figure 10: Cross plot between saturation index and aMg^{2+}/aCa^{2+} indicates that SI_{MHC} higher*
753 *than 1.0 is required for the formation of MHC at aMg^{2+}/aCa^{2+} greater than 2. The data points*
754 *are measurements taken before the precipitation of calcium carbonate. Abiotically*
755 *precipitated calcium carbonate reported in Rodriguez-Blanco et al. (2014) were compared and*
756 *given in square symbols.*

757

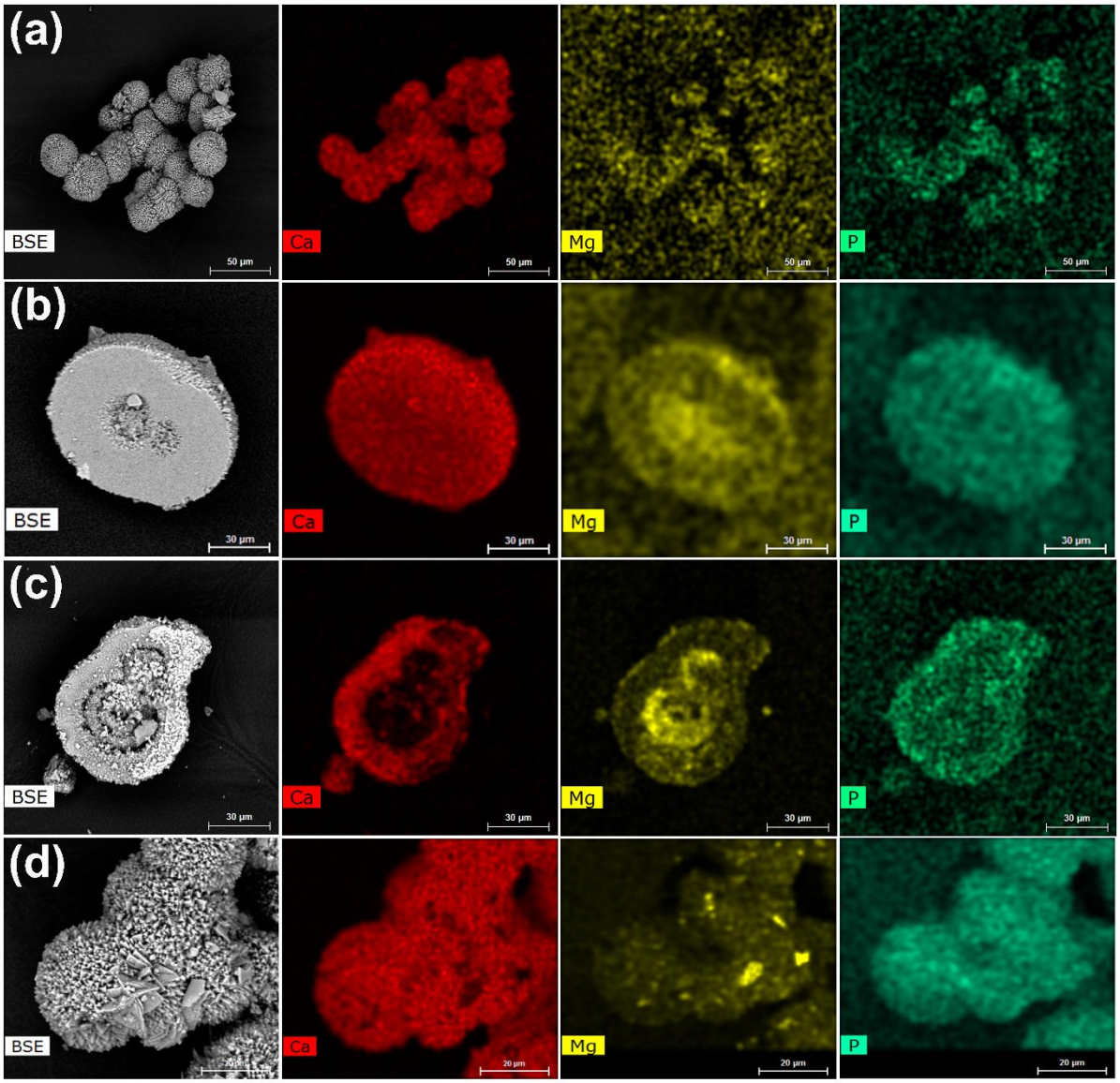

Figure 11: SEM elemental mapping (Ca, Mg and P) of MHC. (a) chemical composition of MHC prior to transformation experiment; (b) hemispherulite MHC with higher Mg distribution at the core prior to transformation; (c) cross section of spherulitic MHC (T-Atl-SW-YE); and (d) surface chemical compositions of MHC (T-Atl-SW-YE) after transformation process.

4.5 The role of microbial sulfate reduction in carbonate polymorphism in the natural environment

Even if MHC forms under the three conditions above in the natural environment, MHC should readily dehydrate and transform into more stable calcium carbonate polymorphs with time. Therefore, we suggest a fourth condition has to be met to find MHC in the natural environment: (4) phosphate and magnesium must be in solution, which we have shown helps

stabilize MHC. This is largely true in anoxic marine sediments which have high magnesium from seawater and high phosphate from the combined effects of organic carbon oxidation and the liberation of adsorbed phosphate from iron-oxide reduction (Hyacinthe and Van Cappellen, 2004). To understand the presence of MHC in natural sediments, we must also constrain the transformation of MHC to stable calcium carbonate polymorphs at low temperatures; in this regard, our laboratory temperatures are warmer than most sedimentary conditions.

In the natural environment, MHC can be formed as a transitional diagenetic phase in the recrystallization process of metastable ikaite to final calcite (Dahl and Buchardt, 2006). The formation of these minerals is often associated with microbial activity, organic materials and the presence of algal mats such as in the sediment of Lake Kivu (Central Africa) (Stoffers and Fischbeck, 1974). Authigenic MHC typically has been found in lacustrine environments, but it also occurs in caves, as weathering products, and fjords (Dahl and Buchardt, 2006). These MHCs are reported to vary in morphology (spherulitic or euhedral) and chemical compositions (variations in magnesium content). For example, several studies have reported the occurrence of spherulitic crystal aggregates in fluid characterized by high organic material and the presence of microorganisms such as microbes and algae (Stoffers and Fischbeck, 1974; Taylor 1975; Teller and Last, 1990; Dahl and Buchardt, 2006). We found close resemblance of some of these naturally-occurring spherulitic MHC with the MHC precipitated in our experiments. This suggests an extended period of supersaturation with respect to MHC in the solution. Nearly all the aqueous phase sample where MHC is forming shared similar geochemical conditions with what we proposed in this study – low temperature, high pH, high alkalinity, high molar Mg/Ca ratios (> 3), and elevated PO_4^{3-} concentration (> 10 μM).

Our results suggest strongly that microbial sulfate reduction drives calcium carbonate precipitation and will influence the carbonate polymorph of the precipitated sedimentary carbonate. If we apply our laboratory experiments to the natural environment, we anticipate sulfate will have a lesser inhibitory effect on sedimentary carbonate formation relative to dissolved phosphate and magnesium. This is partially due to the nucleation effect of the sulfate reducing bacteria, which may counter the inhibition effect of dissolved aqueous sulfate. Nevertheless, we sum the influence of the various variables influencing calcium

carbonate polymorphism via microbial sulfate reduction under a closed system as follow: Mg/Ca >> PO_4^{3-} >> SO_4^{2-}. Although we have demonstrated that microbial sulfate reduction can be directly linked to the formation of MHC and other different calcium carbonate polymorphs, whether microbial sulfate reduction in the environment directly involves in the precipitation of MHC is still unclear. It should be noted that the pore-fluid where these microbes thrive in marine sediment is often characterized by the prerequisite geochemical conditions for MHC to form, such as high alkalinity and the presence of nutrients such as phosphate. The formation of single mineralogy cements can be rare in natural sedimentary systems. Even using pure cultures under controlled conditions, we found mixed mineralogy in some samples (as in sample C-3:1 and C-Alt-SW) that may be due to the unknown growth behavior of the microbes – where the sulfate reducing bacteria re-grew after the first precipitation event (please refer to online supplementary material for detailed growth curve and pH data). The re-growth further increases the alkalinity and led to a second supersaturation but at a much higher Mg/Ca ratio, causing a precipitation of a different calcium carbonate polymorph than the initial precipitation. In closed or semi-closed marine sediment, it is very likely that the growth cycle of microbes might change over time as a function of food source availability, leads to multiple precipitation events and also mixed mineralogy of the precipitated minerals.

5.0 CONCLUSION AND IMPLICATIONS

In conclusion, microbial sulfate reduction is capable of driving precipitation of calcium carbonate polymorphs via metabolic activity that changes the solution chemistry. Bacterial cells can act as effective nucleation surfaces for calcium carbonate polymorphs to grow. The cellular materials are often a better substrate compared to calcite and kaolinite seeds, which likely results from the combined effects of surface energetics and local perturbations to solution chemistry proximal to actively metabolising cells. This also implies that heterogenous precipitation is a dominant precipitation pathway in sediments that host sulfate reducing bacteria. Under a closed and active system, calcium carbonate polymorphs selection depends on the solution chemistry at the time of nucleation, even though the solution chemistry might then evolve. Several variables influence calcium carbonate polymorphism via microbial sulfate reduction under a closed system: Mg/Ca >> PO_4^{3-} >> SO_4^{2-} and the type of seeding materials. The growth of magnesium calcite is promoted in experiments with calcite seeds

834 which, in turn, influences the apparent stability domain between calcite and MHC in the
835 present of calcite and kaolinite seeds. Our biotically-mediated spherulitic MHC comprises a
836 unique hollow cavity with calcified microbial textures. This texture is absent in abiotic
837 experiments, and thus could be useful to interpret biotic sedimentary signatures of
838 precipitated minerals in the environment. Nevertheless, our transformation experiment
839 suggests that such a microbial texture/signature is vulnerable to early diagenetic processes in
840 the environment. Results from biotic, abiotic and transformation experiments showed that
841 phosphate stabilizes MHC, while retarding the formation of aragonite and calcite at Mg/Ca >
842 2. We also found that phosphate concentrations have a lesser effect on which polymorph
843 initially precipitates. In the presence of high phosphate concentrations, MHC formed instead
844 of aragonite because phosphate ions inhibit the nucleation of aragonite. Therefore, we
845 suggest that caution should be taken when interpreting the types of calcium carbonate
846 polymorphs formed in biotic studies that uses yeast extract or any additives that has
847 phosphorus content. Similar claim applies to environmental samples where metastable MHC
848 is particularly prone to diagenetic processes. Thus, care should be taken while interpreting
849 environmental samples as any transformation processes of MHC can have detrimental effect
850 on paleo proxy such as isotopic signature or Mg/Ca in the sedimentary carbonates.
851
852 **ACKNOWLEDGEMENT**
853 The authors would like to acknowledge the funding for this research ERC StG 307582 to AVT
854 (CARBONSINK). CYL would also like to thank the Ministry of Education Malaysia for the SLAI
855 (Skim Latihan Akademik IPTA) scholarship and Universiti Malaya for providing the study leave.
856 The authors are also indebted to Tony Dickson, Harold Bradbury, Gilad Antler, and Jo Clegg
857 for their discussion and assistant in the laboratory.
858
859 **SUPPLEMENTARY MATERIALS**
860
861 **REFERENCES**
862 Aloisi G. Gloter A. Kruger M. Wallmann K. Guyot F. and Zuddas P. (2006) Nucleation of calcium
863 carbonate on bacterial nanoglobules. *Geology* **34**(12), 1017 – 1020.
864 Althoff P.L. (1977) Structural refinements of dolomite and a magnesian calcite and
865 implications for dolomite formation in the marine environment. *Am. Mineral*. **62**, 772 – 783.

Arias D. Cisternas L.A. and Rivas M. (2017) Biomineralization of calcium and magnesium crystals from seawater by halotolerant bacteria isolated from Atacama Salar (Chile). *Desalination*. **405**, 1 – 9.

Balci N. Demirel C. On S.A. Gultekin A.H. Kurt M.A. (2018) Evaluating abiotic and microbial factors on carbonate precipitation in Lake Acigol, a hypersaline lake in Southwestern Turkey. *Quaternary International*. **486**, 116 – 128.

Balci N. Menekse M. Karaguler N.G. Sonmez M.S. and Meister P. (2016) Reproducing authigenic carbonate precipitation in the hypersaline Lake Acigol (Turkey) with microbial cultures. *Geomicrobiol J*. **33**(9), 758 – 773.

Baumgartner L.K. Dupraz C. Buckley D.H. Spear J.B. Pace N.R. and Visscher P.T. (2009) Microbial species richness and metabolic activities in hypersaline microbial mats: Insight into biosignature formation through lithification. *Astrobiol*. **9**(9), 861 – 874.

Berner R.A. Scott M.R. and Thomlinson C. (1970) Carbonate alkalinity in the pore waters of anoxic marine sediments. *Limnol. Oceanography*. **15**(4), 544 – 549.

Berner R.A. (1975) The role of magnesium in the crystal growth of calcite and aragonite from seawater. *Geochim. Cosmochim. Acta*. **39**, 489 – 504.

Berner R.A. and Morse J.W. (1974) Dissolution kinetics of calcium carbonate in seawater. IV. Theory of calcite dissolution. *Am. J. Sci*. **274**, 108 – 134.

Blue C.R. Giuffre A. Mergelsberg S. Han N. De Yoreo J.J. and Dove P.M. (2017) Chemical and physical controls on the transformation of amorphous calcium carbonate into crystalline $CaCO_3$ polymorphs. *Geochim. Cosmochim. Acta*. **196**, 179 – 196.

Bosak T. and Newman D.K. (2005) Microbial kinetic controls on calcite morphology in supersaturated solutions. *J. Sedimentary Res*. **75**(2), 190 – 199.

Bots P. Benning L.G. Rickaby R.E.M. and Shaw S. (2011) The role of SO_4 in the switch from calcite to aragonite seas. *Geology.* **39**, 331 – 334.

Bots P. Benning L.G. Rodriguez-Blanco J.D. Roncal-Herrero R.T. and Shaw S. (2012) Mechanistic insights into the crystallization of amorphous calcium carbonate (ACC). *Crystal Growth Design.* **12**, 3806 – 3814.

Braissant O. Decho A.W. Dupraz C. Glunk C. Przekop K.M. and Visscher P.T. (2007) Exopolymeric substances of sulfate reducing bacteria: Interactions with calcium at alkaline pH and implication for formation of carbonate minerals. *Geobiology*. **5**, 401 – 411.

Brecevic L. and Nielsen A.E. (1989) Solubility of amorphous calcium carbonate. *J. Crystal Growth*. **98**(3), 504 – 510.

Brönsted J.N. (1922) Studies on solubility. IV. The principle of the specific interaction of ions. *J. Am. Chem. Soc*. **44**, 877 – 898.

Brooks R. Clack L.M. and Thurston E.F. (1950) Calcium carbonate and its hydrates. *Phil. Trans. Royal Soc. A*. **243**, 145 – 167.

Burdige D.J. (1991) The kinetics of organic matter mineralization in anoxic marine sediments. *J. Mar. Res*. **49**, 727 – 761.

Burton E.A. and Walter L.M. (1990) The role of pH in phosphate inhibition of calcite and aragonite precipitation rates in seawater. *Geochim Cosmochim Acta*. **54**, 797 – 808.

Burton E.A. (1993) Controls on marine carbonate cement mineralogy: review and reassessment. *Chem Geol*. **105**, 163 – 179.

Busenberg E. and Plummer N.L. (1985) Kinetics and thermodynamic factors controlling the distribution of SO_4^{2-} and Na^+ in calcites and selected aragonites. *Geochim. Cosmochim. Acta*. **49**, 713 – 725.

Chafetz H. Barth J. Cook M. Guo X. and Zhou J. (2018) Origins of carbonate spherulites: Implications for Brazilian Aption pre-salt reservoir. *Sed. Geol*. **365**, 21 – 33.

Chen L. Shen Y. Xie A. Huang B. Jia R. Guo R. and Tang W. (2009) Bacteria-mediated synthesis of metal carbonate minerals with unusual morphologies and structures. *Crystal Growth Design*. **9**(2), 743 – 754.

Christ C.L. and Hostetle P.B. (1970) Studies in system MgO – SiO_2 – CO_2 – H_2O. (II) Activity-product constant of magnesite. *Am. J. Sci*. **268**(5), 439 – 453.

Coelho W.A. (2007) *TOPAS-Academic, Coelho Software*. Brisbane, Australia.

Coleman M.L. Hedrick D.B. Lovley D.R. White D.C. and Pye K. (1993) Reduction of Fe(III) in sediments by sulfate reducing bacteria. *Nature*. **361**, 436 – 438.

Dahl K. and Buchardt B. (2006) Monohydrocalcite in the arctic Ikka Fjord, SW Greenland: First reported marine occurrence. *J. Sedimentary Res*. **76**, 460 – 471.

de Choudens-Sanchez V. and Gonzalez L.A. (2009) Calcite and aragonite precipitation under controlled instantaneous supersaturation: Elucidating the role of $CaCO_3$ saturation state and Mg/Ca ratio on calcium carbonate polymorphism. *J. Sedimentary Res*. **79**, 363 – 376.

De Yoreo J.J. Filbert P.U.P.A. Sommerdijk N.A.J.M. Lee Penn R. Whitelam S. Joester D. Zhang H. Rimer J.D. Navrotsky A. Banfield J.F. Wallace A.F. Michel F.M. Meldrum F.C. Colfen H. and

929 Dove P.M. (2015) Crystallization by particle attachment in synthetic, biogenic, and geologic
930 environments. *Science*. **349**(6247). Doi 10.1126/science.aaa6760.
931 Dejehet F. Idrissi S. and Debuyst R. (1999) Magnesium and occluded water in calcium
932 carbonate monohydrate. *J. de Chimie Physique*. **96**, 741 – 753.
933 Delaney M.L. (1998) Phosphorus accumulation in marine sediments and the oceanic
934 phosphorus cycle. *Global Biogeochem. Cycle*. **12**(4), 563 – 572.
935 Dickson A.G. Afghan J.D. and Anderson G.C. (2003) Reference materials for oceanic CO_2
936 analysis: a method for the certification of total alkalinity. *Mar. Chem*. **80**(2-3), 185 – 197.
937 Dickson J.A.D. (1993) Crystal growth diagrams as an aid to interpreting the fabrics of calcite
938 aggregates. *J. Sedimentary Res*. **63**(1), 1 – 17.
939 Dobberschutz S. Nielsen M.R. Sand K.K. Civioc R. Bovet N. Stipp S.L.S. and Andersson M.P.
940 (2018) The mechanisms of crystal growth inhibition by organic and inorganic inhibitors.
941 *Nature Commun.* **9**, 1578.
942 Dong H. Fredrickson J.K. Kennedy D.W. Zachara J.M. Kukkadapu R.K. and Onstott T.C. (2000)
943 Mineral transformation associated with the microbial reduction of magnetite. *Chem. Geol.*
944 **169**, 299 – 318.
945 Dupraz C. Reid R.P. Braissant O. Decho A.W. Norman R.S. and Visscher P.T. (2009) Processes
946 of carbonate precipitation in modern microbial mats. *Earth Sci. Rev*. **96**, 141 – 162.
947 Egger M. Jilbert T. Behrends T. Rivard C. and Slomp C.P. (2015) Vivianite is a major sink for
948 phosphorus in methanogenic coastal surface sediments. *Geochim. Cosmochim. Acta*. **169**, 217
949 – 235.
950 Elstnerova P. Friak M. Fabritius H.O. Lymperakis L. Hickel T. Petrov M. Nikolov S. Raabe D.
951 Ziegler A. Hild S. and Neugebauer J. (2010) *Acta Biomaterialia*. **6**(10), 4506 – 4512.
952 Faul K.L. Paytan A. and Delaney M.L. (2005) Phosphorus distribution in sinking oceanic
953 particulate matter. *Mar. Chem*. **97**(3 – 4), 307 – 333.
954 Fukushi K. Munemoto T. Sakai M. and Yagi S. (2011) Monohydrocalcite: a promising
955 remediation material for hazardous anions. *Sci. Technol. Adv. Materials*. **12**, 64702 – 64714.
956 Fukushi K. Suzuki Y. Kawano J. Ohno T. Ogawa M. Yaji T. and Takahashi Y. (2017) Speciation of
957 magnesium in monohydrocalcite: XANES, *ab initio* and geochemical modelling. *Geochim.*
958 *Cosmochim. Acta*. **213**, 457 – 474.

959 Gallagher K.L. Kading T.J. Braissant O. Dupraz C. and Visscher P.T. (2012) Inside the alkalinity
960 engine: the role of electron donors in the organomineralization potential of sulfate-reducing
961 bacteria. *Geobiol*. **10**(6), 518 – 530.
962 Gallagher K.L. Braissant O. Kading T.J. Dupraz C. and Visscher P.T. (2013) Phosphate-related
963 artifacts in carbonate mineralization experiments. *J. Sed. Res*. **83**, 37 – 49.
964 Granasy L. Pusztai T. Tegze G. Warren J.A. Douglas J.F. (2005) Growth and form of spherulites.
965 *Phys. Rev. Let*. **72**, 011605.
966 Grases F. and March J.G. (1990) Determination of phosphate based on inhibition of crystal
967 growth of calcite. *Anal. Chim. Acta*. **229**, 249 – 254.
968 Guggenheim E.A. and Turgeon J.C. (1955) Specific interaction of ions. *Trans. Faraday Soc*. **51**,
969 747 – 761.
970 Han Z. Li D. Zhao H. and Yan Li P. (2017) Precipitation of carbonate minerals induced by the
971 halophilic *Chromohalobacter Israelensis* under high salt concentrations: Implications for
972 natural environments. *Minerals*. **7**(6), 95; doi:103390/min7060095.
973 Han M. Zhao Y. Zhao H. Han Z. Yan H. Sun B. Meng R. Zhuang D. Li D. and Liu B. (2017a) A
974 comparison of amorphous calcium carbonate crystallization in aqueous solutions of $MgCl_2$
975 and $MgSO_4$: implications for paleo-ocean chemistry. *Mineral. Petrol*. DOI 10.1007/s00710-
976 017-0528-9. pp 1 – 16.
977 Haouari O. Fardeau M.L. Casalot L. Tholozan J.L. Hamdi M. and Ollivier B. (2006) Isolation of
978 sulfate-reducing bacteria from Tunisian marine sediments and description of *Desulfovibrio*
979 *bizertensis* sp. nov. *Int. J. System. Evol. Microbiol*. **56**, 2909 – 2913.
980 Hood A.V.S. Wallace M.W. and Drysdale R.N. (2011) Neoproterozoic aragonite-dolomite seas?
981 Widespread marine dolomite precipitation in Cryogenian reef complexes. *Geology*. **9**, 871 –
982 874.
983 Hopkinson L. Kristova P. Rutt K. and Cressey G. (2012) Phase transitions in the system MgO-
984 CO_2-H_2O during CO_2 degassing of Mg-bearing solutions. *Geochim. Cosmochim. Acta*. **76**, 1 –
985 13.
986 Hull H. and Turnbull A.G. (1973) A thermodynamic study of monohydrocalcite. *Geochim.*
987 *Cosmochim. Acta*. **37**, 685 – 694.
988 Hyacinthe C. and Van Cappellen (2004) An authigenic iron phosphate phase in estuarine
989 sediments: composition, formation and chemical reactivity. *Mar. Chem*. **91**, 227 – 251.

Ihli J. Wong W.C. Noel E.H. Kim Y.Y. Kulak A.N. Christenson H.K. Duer M.J. and Meldrum F.C. (2014) Dehydration and crystallization of amorphous calcium carbonate in solution and in air. *Nature Comm*. **5**(3169), 1 – 10.

Kamiya K. Sakka S. and Terada K. (1977) Aragonite formation through precipitation of calcium carbonate monohydrate. *Materials Res. Bull*. **12**(11), 1095 – 1102.

Katz A. (1973). The interaction of magnesium with calcite during crystal growth at 25 – 90˚C and one atmosphere. *Geochim. Cosmochim. Acta*. **37**, 1563 – 1586.

Kawaguchi T. and Decho A.W. (2002) A laboratory investigation of cyanobacterial extracellular polymeric secretions (EPS) in influencing $CaCO_3$ polymorphism. *J. Crystal Growth*. **240**, 230 – 235.

Kraal P. Slomp C.P. Reed D.C. Reichart G.J. and Poulton S.W. (2012) Sedimentary phosphorus and iron cycling in and below the oxygen minimum zone of the northern Arabian Sea. *Biogeosciences*. **9**, 2603 – 2624.

Kimura T. and Koga N. (2011) Monohydrocalcite in comparison with hydrated amorphous calcium carbonate: Precipitation condition and thermal behaviour. *Crystal Growth Design*. **11**, 3877 – 3884.

Kipp M.A. and Stueken E.E. (2017) Biomass recycling and Earth's early phosphorus cycle. *Sci. Adv*. **3**, eaao4795, 1 – 6.

Kitson R.E. and Mellon M.G. (1944) Colorimetric determination of phosphorus as molybdivanadophosphoric acid. *Indus. Engin. Chem. Res*. **16**, 379.

Lenders J.J. Dey A. Bomans P.H.H. Spielmann J. Hendrix M.M.R.M. de With G. Meldrum F.C. Harder D. and Sommerdijk N.A.J.M. (2012) High-magnesian calcite mesocrystals: A coordination chemistry approach. *J. Am. Soc*. **134**, 1367 – 1373.

Lippmann F. (1973) *Sedimentary Carbonate Minerals*. Springer Verlag, Berlin Heidelberg.

Lin Y.P. and Singer P.C. (2005) Inhibition of calcite crystal growth by polyphosphates. *Water Res*. **39**(19). 4835 – 4843.

Lin C.J. Yang S.Y. Huang S.J. and Chan J.C.C. (2015) Structural characterization of Mg-stabilized amorphous calcium carbonate by Mg-25 solid-state NMR spectroscopy. *J. Phys. Chem. C*. **119**, 7225 – 7233.

Lioliou M.G. Paraskeva C.A. Koutsoukos P.G. and Payatakes A.C. (2007) Heterogeneous nucleation and growth of calcium carbonate on calcite and quartz. *J. Colloid Interface Sci*. **208**, 421 – 428.

Liu R. Liu F.L. Zhao S.Q. Su Y.L. Wang D.J. and Shen Q. (2013) Crystallization and oriented attachment of monohydrocalcite and its crystalline phase transformation. *Cryst. Engin. Comm*. **15**, 509 – 515.

Loste E. Wilson R.M. Seshadri R. and Meldrum F.C. (2003) The role of magnesium in stabilizing amorphous calcium carbonate and controlling calcite morphologies. *J. Crystal Growth*. **254**, 206 – 218.

Madsen I.C. and Scarlett N.V.Y. (2008) Quantitative Phase Analysis. In *Powder Diffraction: Theory and Practice* (eds by Dinnabier, R.E.). Royal Society of Chemistry.

Marschner H. (1969) Hydrocalcite ($CaCO_3.H_2O$) and Nesquehonite ($MgCO_3.3H_2O$) in carbonate scales. *Science*. **165**, 1119 – 1121.

McCusker L.B. Von Dreele R.B. Cox D.E. Louer D. Scardi P. (1999) Reitveld refinement guidelines. *J. Appl. Crystallography*. **32**(1), 36 – 50.

Meic I.B. Kontec J. Jurasin D.D. Dzakula B.N. Stajner L. Lyons D.M. Sikiric M.D. and Kralj D. (2017) Comparative study of calcium carbonates and calcium phosphates precipitation in model systems mimicking the inorganic environment for biomineralization. *Crystal Growth Design*. **17**(3), 1103 – 1117.

Meister P. (2013) Two opposing effects of sulfate reduction on carbonate precipitation in normal marine, hypersaline, and alkaline environments. *Geology*. **41** (4), 499 – 502.

Morse J.M. and He S. (1993) Influences of T, S and P_{CO2} on the pseudo-homogeneous precipitation of $CaCO_3$ from seawater: implications for whiting formation. *Mar. Chem*. **41**, 291 – 297.

Munemoto T. and Fukushi K. (2008) Transformation kinetics of monohydrocalcite to aragonite in aqueous solutions. *J. Mineral. Petrol. Sci*. **103**, 345 – 349.

Munemoto T. Fukushi K. Kanzaki Y. and Murakami T. (2014) Redistribution of Pb during transformation of monohydrocalcite to aragonite. *Chem. Geol*. **387**, 133 – 143.

Nishiyama R. Munemoto T. and Fukushi K. (2013) Formation condition of monohydrocalcite from $CaCl_2$-$MgCl_2$-Na_2CO_3 solutions. *Geochim. Cosmochim. Acta*. **100**, 217 – 231.

Nielsen M.R. Sand K.K. Rodgriguez-Blanco J.D. Bovet N. Generosi J. Dalby K.K. and Stipp S.L.S. (2016) Inhibition of calcite growth: Combined effects of Mg^{2+} and SO_4^{2-}. *J. Crystal Growth*. **16**, 6199 – 6207.

1052 Nyiro-Kosa I. Rostasi A. Bereczk-Tompa E. Cora I. Koblar M. Kovacs A. and Posfai M. (2018)
1053 Nucleation and growth of Mg-bearing calcite in a shallow, calcareous lake. *Earth Planet. Sci.*
1054 *Lett.* **496**, 20 – 28.
1055 Obst M. Dynes J.J. Lawrence J.R. Swerhone G.D.W. Benzerara K. Karunakaran C. Kaznatcheev
1056 K. Tyliszczak T. and Hitchcock A.P. (2009) Precipitation of amorphous $CaCO_3$ (aragonite-like)
1057 by cynobacteria: A STXM study of the influence of EPS on the nucleation process. *Geochim.*
1058 *Cosmochim. Acta*. **73**, 4180 – 4198.
1059 Omoike A. and Chorover J. (2006) Adsorption to goethite of extracellular polymeric
1060 substances from *Bacillus subtilis*. *Geochem. Cosmochim. Acta*. **70**, 827 – 838.
1061 Oomori T. Kyan A. and Kitano Y. (1988) Magnesium calcite synthesis from calcium bicarbonate
1062 solution containing magnesium ions in the presence of fluoride and phosphate ions. *Geochem.*
1063 *J*. **22**, 275 – 283.
1064 Picard A. Gartman A. Clarke D.R. and Girguis P.R. (2018) Sulfate-reducing bacteria influence
1065 the nucleation and growth of mackinawite and greigite. *Geochim. Cosmochim. Acta*. **220**, 367
1066 – 384.
1067 Plummer L.N. and Busenberg E. (1982) The solubilities of calcite, aragonite and vaterite in CO_2
1068 – H_2O solutions between 0 and 90˚C, and an evaluation of the aqueous model for the system
1069 $CaCO_3$-CO_2-H_2O. *Geochim. Cosmochim. Acta*. **46**(6), 1011 – 1040.
1070 Politi Y. Arad T. Klein E. Weiner S. and Addadi L. (2004) Sea urchin spine calcite forms via a
1071 transient amorphous calcium carbonate phase. *Science.* **306**, 1161 – 1164.
1072 Purgstaller B. Konrad F. Dietzel M. Immenhauser A. and Mavromatis V. (2017) Control of
1073 Mg^{2+}/Ca^{2+} activity ratio on the formation of crystalline carbonate minerals via an amorphous
1074 precursor. *Crystal Growth Design*. **17**, 1069 – 1078.
1075 Pye K. Dickinson A.D. Schiavon N. Coleman M.L. and Cox M. (1990). Formation of siderite-Mg-
1076 calcite iron sulphide concretions in intertidal marsh and sandflat sediments, north Norfolk,
1077 England. *Sedimentology*. **37**, 325 – 343.
1078 Qiu X. Yao Y. Wang H. and Duan Y. (2017) Live microbial cells adsorb Mg^{2+} more effectively
1079 than lifeless organic matter. *Frontiers Earth Sci*. DOI 10.1007/s11707-017-0626-3.
1080 Raiswell R. and Fisher Q.J. (2004) Rates of carbonate cementation associated with sulfate
1081 reduction in DSDP/ODP sediments: Implications for the formation of concretions. *Chem. Geol*.
1082 **211**, 71 – 85.

1083 Ries J.B. Anderson M.A. and Hill R.T. (2008) Seawater Mg/Ca controls polymorph mineralogy
1084 of microbial $CaCO_3$: A potential proxy for calcite-aragonite seas in Precambrian time.
1085 *Geobiology*. **6**, 106 – 119.
1086 Rivadeneyra M.A. Delgado G. Ramos-Cormenzana A. and Delgado R. (1998) Biomineralization
1087 of carbonates by *Halomonas eurihalina* in solid and liquid media with different salinities:
1088 crystal formation sequence. *Res. Microbiol*. **149**(4), 227 – 287.
1089 Rivadeneyra M.A. Martin-Algarra A. Sanchez-Roman M. Sanchez-Navas A. Martin-Ramos J.D.
1090 (2010) Amorphous Ca-phosphate precursors for Ca-carbonate biominerals mediated by
1091 Chromohalobacter marismortui. *ISME J*. **4**, 922 – 932.
1092 Rodriguez-Blanco J.D. Shaw S. Bots P. Roncal-Herrero T. Benning L.G. (2014) The role of Mg in
1093 the crystallization of monohydrocalcite. *Geochim. Cosmochim. Acta*. **127**, 204 – 220.
1094 Rodriguez-Navarro C. Jroundi F. Schiro M. Ruiz-Agdo E. and Gonzalez-Munoz M.T. (2012)
1095 Influence of substrate mineralogy on bacterial mineralization of calcium carbonate:
1096 Implications for stone conservation. *Appl Environ Microbiol*. **78** (11), 4017 – 4029.
1097 Rodriguez-Blanco J.D. Sand K.K. and Benning L.G. (2017) ACC and vaterite as intermediates in
1098 the solution-based crystallization of $CaCO_3$. In A.E.S. Van Driessche et al. (eds.), *New*
1099 *Perspectives on Mineral Nucleation and Growth.* DOI10.1007/978-3-319-45669-0_5.
1100 Sanchez-Navas A. Martin-Algarra A. Rivadeneyra M.A. Melchor S. Martin-Ramos J.D. (2009)
1101 Crystal-growth behaviour in Ca-Mg carbonate bacterial spherulites. *Crystal Growth Design*.
1102 **9**(6), 2690 – 2699.
1103 Sanchez-Roman M. Rivadeneyra M.A. Vasconcelos C. McKenzie J.A. (2007) Biomineralization
1104 of carbonate and phosphate by moderately halophilic bacteria. *FEMS Microbiol. Ecol*. **61**, 273
1105 – 284.
1106 Sasaki K. Noriki S. and Tsunogai S. (2001) Vertical distributions of interstitial phosphate and
1107 fluoride in anoxic sediment: Insight into the formation of an authigenic fluoro-phosphorus
1108 compound. *Geochem. J*. **35**, 295 – 306.
1109 Sinkko H. Lukkari K. Sihvonen L.M. Sivonen K. Leivuori M. Rantanen M. Paulin L. and Lyra C.
1110 (2013) Bacteria contribute to sediment nutrient release and reflect progressed eutrophication
1111 driven hypoxia in an organic-rich continental sea. *PLoS ONE*. **8**(6), e67061.
1112 Doi:10.1371/journal.pone.0067061.

1113 Smeets P.J.M. Cho K.R. Kempen R.G.E. Sommerdijk N.A.J.M. and De Yoreo J.J. (2015) Calcium
1114 carbonate nucleation driven by ion binding in a biomimetic matrix revealed by *in situ* electron
1115 microscopy. *Nature Materials*. **14**, 394 – 399.
1116 Soetaert K. Hofmann A. Middleberg J. Meysman F. and Greenwood J. (2007). The effect of
1117 biogeochemical processes on pH. *Mar. Chem*. **105**, 30 – 51.
1118 Steiner Z. Rapaport H. Oren Y. and Kasher R. (2010) Effect of surface-exposed chemical groups
1119 on calcium-phosphate mineralization in water treatment system. Env. Sci. Technol. **44**, 7937
1120 – 7943.
1121 Stockmann G. Tollefsen E. Skelton A. Bruchert V. Balic-Zunic T. Langhof J. Skogby H. and
1122 Karlsson A. (2018) Control of a calcite inhibitor (phosphate) and temperature on ikaite
1123 precipitation in Ikka Fjord, southwest Greenland. *Appl. Geochem.* **89**, 11 – 22.
1124 Stoffers P. and Fischbeck R. (1974) Monohydrocalcite in the sediments of Lake Kivu (East
1125 Africa). *Sedimentology*. **21**, 163 – 170.
1126 Sun W. Jayaraman S. Chen W. Persson K.A. and Ceder G. (2015) Nucleation of metastable
1127 aragonite $CaCO_3$ in seawater. *Proc. Nat. Acad. Sci*. **112**(11), 3199 – 3204.
1128 Suzuki M. Nagasawa H. and Kogure T. (2006) Synthesis and structure of hollow calcite particles.
1129 *Crystal Growth Design*. **6**(9), 2004 – 2006.
1130 Tadier S. Rokidi S. Rey C. Combes C. and Koutsoukos P.G. (2017) Crystal growth of aragonite
1131 in the presence of phosphate. *J. Crystal Growth*. **458**, 44 – 52.
1132 Taylor G.F. (1975) The occurrence of monohydrocalcite in two small lakes in the South-East
1133 of South Australia. *Am. Mineral*. **60**, 690 – 697.
1134 Teller J.T. and Last W.M. (1990) Paleohydrological indicators in playas and salt lakes, with
1135 examples from Canada, Australia, and Africa. *Paleogeo. Paleoclim. Paleoecol*. **76**, 215 – 240.
1136 Tracy S.L. Williams D.A. and Jennings H.M. (1998) The growth of calcite spherulites from
1137 solution II. Kinetics of formation. *J. Crystal Growth*. **193**, 382 – 388.
1138 Tommaso D.D. and de Leeuw N.H. (2010) Structure and dynamics of the hydrated magnesium
1139 ion and of the solvated magnesium carbonates: insights from first principles simulations. *Phys.*
1140 *Chem. Chem. Phys*. **12**, 894 – 901.
1141 Tourney J. and Ngwenya B.T. (2009) Bacterial extracellular polymeric substances (EPS)
1142 mediate $CaCO_3$ morphology and polymorphism. *Chem. Geol*. **262**, 138 – 146.
1143 van Lith Y. (2001) *The role of sulfate reducing bacteria in dolomite formation. Study of a recent*
1144 *environment, bacterial cultures, and dolomite concretions*. PhD thesis.

1145 Visscher P.T. Reid R.P. and Bebout B.M. (2000) Microscale observations of sulfate reduction:
1146 Correlation of microbial activity with lithified micritic laminae in modern marine stromatolites.
1147 *Geology*. **28**(10), 919 – 922.
1148 Visscher P.T. and Stolz, J.F. (2005) Microbial mats as bioreactors: Populations, processes, and
1149 products. *Paleogeo. Paleoclim. Paleoecol*. **219**, 87 – 100.
1150 Wacey D. Wright D.T. and Boyce A.J. (2007) A stable isotope study of microbial dolomite
1151 formation in the Coorong Region, South Australia. *Chem. Geol*. **244**, 155 – 174.
1152 Walter L.M. (1986) Relative efficiency of carbonate dissolution and precipitation during
1153 diagenesis: a progress report on the role of solution chemistry. In Gautier, D.L., ed., *Roles of*
1154 *organic matter in sediment diagenesis*: Soc. Econ. Pal. Min. Sp. Pub. 38, p. 1 – 11.
1155 Walter L.K. and Burton E.A. (1986) The effect of orthophosphate on carbonate mineral
1156 dissolution rates in seawater. *Chem. Geol*. **56**, 313 – 323.
1157 Warthmann R. van Lith Y. Vasconcelos C. McKenzie J.A. and Karpoff A.M. (2000) Bacterially
1158 induced dolomite precipitation in anoxic culture experiments. *Geology*. **28**(12), 1091 – 1094.
1159 Wolf S.L. Jahme K. and Gebauer D. (2015) Synergy of Mg^{2+} and poly(aspartic acid) in additive-
1160 controlled calcium carbonate precipitation. *Cryst. Engin. Comm*. **17**, 6857 – 6862.
1161 Xu J. Yan C. Zhang F. Konishi H. Xu H. and Teng H.H. (2013) Testing the cation-hydration effect
1162 on the crystallization of Ca-Mg-CO_3 systems. *Proc. Nat. Acad. Sci.* **110**(44), 17750 – 17755
1163 Yagi S. and Fukushi K. (2011) Phosphate sorption on monohydrocalcite. *J. Mineral. Petrol. Sci.*
1164 **106**, 109 – 113.
1165 Zhu, T. and Dittrich M. (2016) Carbonate precipitation through microbial activities in natural
1166 environment, and their potential in biotechnology: A review. *Frontiers Bioengin. Biotechnol*.
1167 **4**(4), 1 – 21.